ATOMIC FLUORESCENCE IN A PULSED HOLLOW CATHODE DISCHARGE WITH A COPPER VAPOR PUMPED DYE LASER

BY

JAMES BENJAMIN WOMACK

A DISSERTATION PRESENTED TO THE GRADUATE SCHOOL
OF THE UNIVERSITY OF FLORIDA IN PARTIAL FULFILLMENT
OF THE REQUIREMENTS FOR THE DEGREE OF
DOCTOR OF PHILOSOPHY

UNIVERSITY OF FLORIDA

1991

Dedicated to my parents and grandparents, who made the impossible seem possible, and to my friends, who made the impossible seem probable.

ACKNOWLEDGEMENTS

The author gratefully acknowledges the support of Cheryl Morgan, Edison Becerra, and, especially, Dr. Benjamin Smith; their contribution to this work was thoughtfully appreciated.

I would like to thank the members of Dr. Winefordner's research group, past and present. I would like to especially mention Dr. Jorge Vera and Dr. Mark Glick for sharing their technical knowledge and Dr. Anthony Mellone for his friendship.

Many personal thanks go to Eric Gessler, without whose enthusiasm for the project, technical support, and personal friendship this would not have been possible.

Personal thanks go to the division secretaries, Jeanne Karably and Susan Ciccarone, for their personal friendship and technical support; to Rudy in the glass shop; to Chester, Vern, and the rest of the machine shop; and to Steve and Mark in the electronics shop.

I would most especially thank Sharon Strain for her professional and personal contribution to this work. Her unending patience, moral support, and good humor were invaluable. I thank you, Shari.

Final acknowledgements go with my utmost thanks to Dr. James D. Winefordner. The opportunity to be a part of the best spectroscopy group in the world and to work with such a distinguished and friendly individual was the highlight of my academic career.

TABLE OF CONTENTS

LIST OF TABLES

LIST OF FIGURES

Abstract of Dissertation Presented to the
Graduate School of the University of Florida in
Partial Fulfillment of the Requirements for
the Degree of Doctor of Philosophy

ATOMIC FLUORESCENCE IN A PULSED HOLLOW CATHODE DISCHARGE WITH A COPPER VAPOR PUMPED DYE LASER

by

James B. Womack

January 7, 1991

Chairman: James D. Winefordner
Major Department: Chemistry

Application of a pulsed glow discharge as an atomizer for atomic fluorescence spectroscopy with a copper vapor pumped dye laser excitation source was investigated. The discharge system was synchronously pulsed with the laser to enable the fluorescence measurement to occur in the low noise background between discharge pulses. This improved the signal to noise significantly over non-pulsed glow discharges. The low pressure, inert gas atmosphere insured an almost ideal environment for fluorescence measurement. The high repetition rate of the pulsed copper vapor laser (6000 Hz) improved the detection efficiency over lower repetition rate laser systems by increasing the probing rate. Disposable graphite cup electrodes were used as demountable hollow cathodes for measurement of aqueous samples. The samples were injected into the cathode cups and dried using a programmable

electrothermal device for reproducibility. The discharge chamber was a commercially available vacuum chamber adapted for both flowing and static gas environments. Operational parameters, such as chamber pressure, discharge voltage, sample volume, cathode cup diameter, and laser-glow discharge pulse synchronization, were evaluated for maximum fluorescence signal. Calibration curves were obtained for lead, iridium, gallium, iron, and cobalt and a determination of lead concentration in standard estuarine river sediment was performed. The detection limits for these elements were in the femtogram to picogram range. The determination of lead in the estuarine river sediment provided percent relative standard deviations of between 2.5 and 2.8. The determination of optimum operational parameters of the glow discharge gave mixed results. It was found that the optimum chamber pressure was 10 torr, the optimum injected sample volume was between 2 and 40 μL, the optimum cathode size was the smaller of the two used, and an interdependence of the optimum glow discharge voltage and laser-glow discharge pulse synchronization was discovered. The results of these determinations and the optimum glow discharge operational parameter data will be presented in this dissertation along with brief sections on the experimental, historical, and theoretical aspects pertinent to the method.

CHAPTER 1
INTRODUCTION

In the last decade, a tremendous emphasis has been placed on the need for ultratrace analysis of metals in a variety of samples ranging from nuclear and biological, to electronics and semiconductor materials. Recent advances in the production and use of high purity materials in today's technology as well as a new understanding of the role of trace metals in biological systems have forced analytical chemists to seek new methods of analysis with greatly increased sensitivities. Research in new analytical technologies is therefore imperative in light of today's analytical needs in the fields of materials, biological, and environmental sciences.

In order to understand the difficulty of this type of analysis one must define the term "ultratrace" analysis. In the analysis of a sample, the constituent of interest can have a broad concentration range. Constituents are classified as "trace" when they are present in amounts lower than 0.01% (100 $\mu g\ g^{-1}$). The amount of the sample used in the analysis is also used as a basis for classification. When the sample size is lower than 10^{-4}g it is considered an "ultramicro" sample. The determination of trace constituents in an ultramicro sample is thus termed an "ultratrace" analysis [1]. To put these terms into numbers, an ultratrace analysis of a constituent would need an analytical method with enough sensitivity to achieve

concentration detection limits ranging from 0.1 ng g^{-1} to 0.1 pg g^{-1} which correspond to absolute detection limits in the 0.1 pg to 0.1 fg range.

Need for Ultratrace Sensitivity

An excellent example of a need for this type of analysis is the determination of dopant impurities in semiconductor materials. In the chemical doping of the silicon substrate, it is desirable to introduce the dopant with as few metal impurities as feasible. This is due to the potential electrical activity in the forbidden band and consequential performance degradation even at the atomic level that contaminant metals such as aluminum (Al), calcium (Ca), cobalt (Co), molybdenum (Mo), zinc (Zn), etc. cause. The ultratrace analysis of these dopant impurities is therefore imperative for dopant purity evaluation and verification [2]. Sensitivities required for this range from 0.1 ng g^{-1} to 0.1 pg g^{-1}. Therefore if 1 mg of homogeneous sample can be analyzed, the absolute detection limits needed would be in the 0.1 pg to 0.1 fg range.

Another example of the need for ultratrace analysis is the toxicological study of thallium poisoning. While elevated levels of thallium are easily detectable by conventional methods, naturally occurring levels of thallium in biological tissues are below the detection limits of most analytical methods. Methods routinely used for thallium determination in biological tissues include: spark source and field desorption mass spectrometry, anodic stripping voltametry, ICP emission spectrometry, and both flame and graphite furnace atomic absorption spectrometry. Since naturally occurring levels must be known to establish a control for toxicological

studies, preconcentration techniques have been used in the past [3-7]. This technique suffers from both increased analysis time and, more importantly, increased matrix effects. The availability of an analytical technique which could analyze thallium at its naturally occurring levels in the pg g^{-1} to ng g^{-1} range would be quite valuable.

Laser Excited Atomic Fluorescence for Ultratrace Sensitivity

While the upper detection limit of ultratrace analysis can be approached by several analytical techniques, very few are capable of approaching absolute detection limits in the femtogram range needed. Of these few techniques, only laser-based atomic spectrometry methods offer a viable approach to routine ultratrace analysis. These methods encompass such spectrometry techniques as laser-enhanced ionization and laser-excited fluorescence. Research emphasis has been placed heavily in the past few years on these two methods in order to provide the analytical chemist with the technology for routine ultratrace analysis as well as in hopes of achieving the ultimate goal of single atom detection [8-11].

The use of laser-excited atomic fluorescence spectrometry (LEAFS) to achieve ultratrace levels of sensitivity has been well documented. An example of its usefulness can be found in the previously mentioned determination of thallium in biological tissues. A LEAFS-based method was developed utilizing graphite furnace atomization which was capable of detecting thallium concentrations well below the naturally occurring levels [12]. An instrumental absolute detection limit of 6 fg of thallium was obtained with this method.

Because of its ability as an ultratrace analysis technique, research on LEAFS is continuing to increase its sensitivity and utility. The LEAFS method is based on the phenomenon of atomic fluorescence which is the optical excitation of atoms to an excited state which subsequently undergo radiational deexcitation over a short period of time. It is this deexcitation radiation that is termed fluorescence. Atomic fluorescence can be classified into two major categories. If the fluorescent photon is the same energy as the excitation photon, it is said to be resonance fluorescence. If the fluorescence photon is of a different energy it is said to be nonresonance fluorescence. Nonresonance fluorescence is almost exclusively preferred because it gives the practical advantage of being able to differentiate between the excitation light and the fluorescent light on the basis of energy or wavelength discrimination to reduce source scatter to the detector. This reduction of scattered source light is very important in improving the sensitivity of the method. These two major categories are subdivided into many individual subcategories based on the type of absorptive and fluorescent energy transitions the atom undergoes [13].

Several types of light sources can be used for atomic fluorescence excitation. These include hollow cathode lamps, electrodeless discharge lamps, metal vapor discharge lamps, xenon arc lamps, inductively coupled plasmas (ICPs), and most recently, lasers. Only tunable pulsed dye lasers currently have sufficient irradiance and tunability to achieve practical ultratrace LEAFS. This is because their use brings about a number of advantages. Foremost among these is their high irradiance which allows optical saturation of the fluorescence transition making the fluorescence

transition dependent on the atom's own properties and more independent of its environment. Other advantages include the wide range of wavelengths now covered by dye lasers and their ability to obtain temporal resolution. However, because of their high source irradiance, they can only be used for nonresonance fluorescence because of the intense source scatter.

The Glow Discharge as an Atomizer

Several types of atomizers have been traditionally used to atomize samples for atomic fluorescence spectrometry. These atomizers usually operate on the principle of thermal atomization and include heated vapor cells, flames, ICPs and graphite furnaces. Flames were the first atomizer to be used for analytical spectrometry but suffer from a compromise between atomization efficiency and fluorescence quenching. Scattering from unvaporized solute particles can be a problem also. ICPs offer much better quantum efficiency (lower quenching) due to the inert argon (Ar) atmosphere and better atomization efficiency due to its higher temperature (typically 3000-3500 K in the viewing region). The disadvantages of ICPs include high background emission and ionic fluorescence spectral interference.

Both of the above atomizer systems suffer from a common disadvantage of requiring relatively large amounts of sample because of the need for continuous aspiration into the atomizer. This can be a major stumbling block when only small amounts of samples are available such as in forensic analysis. One atomizer needing only small samples (1 μL or less) is the electrothermal or graphite furnace atomizer. This atomizer also has the highest atomization efficiency of those currently in use

and therefore the best absolute detection limits. Electrothermal atomizers (ETAs) also have an inert atmosphere (Ar) which reduces quenching. Disadvantages of the graphite furnace include significant analyte interferences, scattering and blackbody emission in the visible region. Another disadvantage of ETAs is related to their rapid atomization of the small sample. Atomization of the sample is usually complete in two to three seconds. This short time period allows little time to tune the source to the desired transition and optimize the fluorescence detection and collection system. To circumvent this an ancillary tuning apparatus such as a separate flame is usually included in the system. This is not needed for laser fluorescence in flames and ICP cells, where analyte can be continuously introduced into the sample atomizer to allow tuning and optimization. It is these disadvantages which make research into new atomizer technology imperative in the continuing development of LEAFS for practical ultratrace analysis.

Recently low pressure discharges have been used as atomization sources for atomic fluorescence spectrometry. A low pressure or "glow" discharge occurs when two electrodes, an anode and a cathode, are surrounded by a low pressure gas (usually an inert gas) while a potential is held across them. Typical operating parameters are between 0.1 and 20 torr pressure and between 200 and 1600 V potential. This type of atomizer operates on the principle of physical sputtering instead of thermal processes and is therefore independent of the thermal properties of the sample. The low pressure inert gas environment provides an almost ideal situation for fluorescence measurement. The low pressure reduces pressure

broadening and the inert gas reduces fluorescence quenching. This type of environment also reduces compound formation and virtually eliminates sample matrix effects. Glow discharge devices require only small samples and even though discreet samples are used, the atomization time is sufficient to allow all tuning and optimization to be done using no other ancillary devices. When operated with a hollow cathode geometry the atoms are confined to a small area which improves the probing efficiency. These properties make the glow discharge attractive as an atomizer for atomic fluorescence spectrometry.

The glow discharge does suffer from several disadvantages; however, that must be addressed. The sputtering atomization rate is low compared to other atomizers, especially ETAs. The glow discharge is extinguished by water and therefore complicates the handling of aqueous samples. Finally, the background emission from a glow discharge is sufficiently intense to enable them to be routinely used as light sources for optical spectrometry (hollow cathode lamps).

To circumvent this high background emission, the glow discharge is pulsed synchronously with a pulsed dye laser, which enables one to time the excitation laser pulse to coincide with the low emission dark period between discharge pulses. One can then observe the fluorescence in a low noise background and significantly improve the signal to background ratio of the system. This is made possible because significant atom population density exists for several milliseconds after the discharge pulse while emission disappears after around 5 μs [14].

Intent of Dissertation

The present work was performed to evaluate a pulsed glow discharge device for use as an atomizer for laser excited atomic fluorescence spectrometry with a copper vapor-dye laser system. The evaluation of this system involved determining optimal operational parameters for the atomizer such as vacuum chamber pressure, sample size, cathode cup diameter, discharge operating voltage, and the timing of the laser pulse with respect to the discharge pulse. Once these optimum parameters were determined, the analytical usefulness of the system was investigated by developing an analytical method for the measurement of several elements, including lead (Pb), iridium (Ir), iron (Fe), cobalt (Co), and gallium (Ga).

CHAPTER 2
HISTORICAL DEVELOPMENTS

The Development of Atomic Fluorescence Spectrometry

The theory of the re-emission of light by an atom was developed in the late 1890s. Scientists knew that classical theory predicted that Na should emit as well as absorb its characteristic D-line radiation [15-19]. Studies to prove this experimentally were undertaken by Wood in 1903 [20] and by Wiedeman and Schmidt [21] but proved to be unsuccessful. Success was finally achieved by Wood in 1905 by vaporizing Na in an evacuated tube and illuminating it with a gas flame aspirating a solution of NaCl [22, 23]. Wood termed this re-emission of light "resonance" radiation. Experiments were continued in vapor cells on volatile elements by Wood, Terennin, Strutt, Christenson, and Rolofson in the following 20 years. Also during this period experiments were carried out using a furnace-generated atomic beam as an atom source by Dunoyer and Bogras. Excellent reviews of this early research are available by Pringsheim [24], and by Mitchell and Zemanskii [25]. Flames were first used as atomization sources by Nichols and Howes in 1923 [26] and were also described in a classic paper by Badger [27]. Most of this work investigated basic atomic spectra.

Research interest in atomic fluorescence waned after the early 1930s and did not resurface again until the middle 1950s with work by Boers, Alkemade, and Smit

who studied quenching processes in flames [28]. The first consideration to using atomic fluorescence for quantitative purposes was given by Alkemade in 1962 [29]. Following this suggestion Winefordner, Vickers, and Staab reported the first use of atomic fluorescence as a quantitative technique in 1964 [30, 31]. The measurement of Ca, mercury (Hg), and Zn was accomplished using a total consumption burner as an atomizer with excitation provided by a low intensity metal vapor discharge (OSRAM) lamps. The method was further optimized by Winefordner, Mansfield, and Veillon in 1964 [32]. Subsequent developments that followed included fluorescence optimized flames and nebulizers, continuum sources, electrothermal atomizers, ICPs as both atomizers and sources, electrodeless discharge lamps and hollow cathode lamps as sources, and improved measuring systems such as boxcar averagers, phase sensitive amplifiers, image detectors, and photon counting. More detailed information on the development of this technique can be found in monographs by Winefordner, Schulman, and O'Haver [33]; Syrenka, Svoboda, and Rubeska [34]; and Kirkbright and Sargent [35]. There are a large number of reviews on the subject also [36-50].

One of the developments most pertinent to the use of atomic fluorescence for ultratrace analysis was the development of the use of lasers as high intensity excitation sources. This was first reported by Fraser and Winefordner in 1971 [51]. Here a nitrogen-pumped tunable dye laser was used with a nebulizer-burner atomization system. Detection limits for Al, Ca, chromium (Cr), Fe, Ga, indium (In), manganese (Mn), strontium (Sr), and titanium (Ti) were reported and were 10 to 100

times better than those with conventional sources. Denton and Malmstadt presented simultaneously and independently a similar experiment [52]. The main advantage of using a laser excitation source is the ability of the source to saturate the fluorescence transition upper energy level. Several papers report the attainment of saturation conditions using laser pumping in the early 1970s [53-58].

The Development of Atomizer System Technology

Atomizer technology for quantitative technology had its beginning with the total consumption flame that was used by Winefordner and Staab. Because these flames were noisy and inefficient atomizers, separated flames began to be used soon after the introduction of the technique. These flames used an inert gas shield to prevent the entrainment of the surrounding atmosphere and the oxygen it contained into the flame gases. This created a more favorable environment for fluorescence measurement [1]. Other flames used were premixed laminar flow burners and turbulent flow burners, and research into different combustion gases was conducted also [59].

In the search for more efficient sample atomization electrothermal atomizers (ETAs) were also investigated. The first attempt by Svoboda [60] to observe fluorescence of a sample atomized by an ETA proved unsuccessful. The first truly useful graphite furnace ETA was designed by Massmann [61, 62] which was a graphite cup with two slots cut in the walls to allow the excitation radiation in and to view the fluorescence radiation at right angles. The cup was placed in a holder which served as the electrical connections and was surrounded by an argon

atmosphere. A similar graphite furnace was introduced by Fraser [63]. Other pioneers in this field were Bolshov, Zybin, and Smirenkena [64]; Dougherty, Preli, and Michel [65]; and Falk, Paetzold, Schmidt, and Tisch [66]. A commercial type of device was used by Goforth and Winefordner with laser excitation in the early 1980s with excellent results [67]. A major factor in the success of ETAs when used with laser excitation was the advent of the pierced mirror optical collection system by Goforth and Winefordner [68], and Omenetto et al. [69]. This device consisted of a mirror which had a small center aperture to allow the laser beam into the furnace tube and which subsequently directed the fluorescent light at right angles to the laser beam onto the slit of a monochromator-detector system (see Figure 2-1). This type of system coupling laser excitation with electrothermal atomization offers the best sensitivity of any of the LEAFs systems [70].

Another type of atomizer which received some research attention was the inductively coupled plasma (ICP). The first use of an ICP as an atomizer cell for atomic fluorescence spectroscopy (AFS) was by Montaser and Fassel [71]; they used electrodeless discharge lamps to excite atomic fluorescence from cadmium (Cd), Hg and Zn in a conventional plasma. Research continued in the use of ICP atomizers by such groups as Demers and Alemand [72], Epstein, Nikdel, Omenetto, Reeves, and Winefordner [73], and others [74]. So successful was the ICP atomizer with hollow cathode lamp excitation that a commercial AFS instrument was offered by a major manufacturer. Research into the ICP as an atomizer for LEAFS continues today with its use for the determination of rare earth metals.

Figure 2-1. Schematic of Optical Layout of Pierced Mirror Fluorescence Collection System with a Graphite Furnace Atomizer. From Goforth and Winefordner [68].

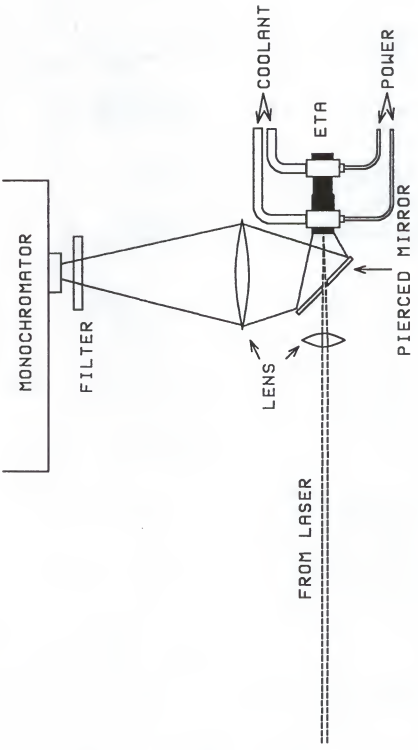
MONOCHROMATOR
FILTER
LENS
FROM LASER
COOLANT
ETA
POWER
PIERCED MIRROR

Other atomizers have also been used for AFS such as hot wire loops, platinum furnaces, introduction by hydride generation and other more esoteric methods.

The Glow Discharge

The conduction of electricity through a gas (electrical discharges) has long been known to occur in nature. Several natural phenomena are closely related to electrical or glow discharge events. Examples of this include lightning, St. Elmo's fire, and the aurora borealis, or northern lights. Electrical discharges were first studied scientifically by Gilbert in his work on gaseous conduction called "de Magnete," published in 1600 and later studied by Coulomb in 1785. The scientific development of glow discharge research closely followed the advancement of vacuum and high voltage technologies. Subsequent research followed between 1850 and 1900 by Crookes, Hittorf, Goldstein, and Hertz. The major impetus of this work was the evaluation of planar electrode discharges developed by Geisler and subsequently called Geisler tubes. At the turn of the century, progress was made with the discovery of x-rays by Roentgen in 1896, the work of Thompson with low pressure discharge tubes which led to the discovery of the electron, and the work by Thompson and Aston on the mass spectrometry of ions [75].

A major development was made by Paschen in 1916 [76, 77], who constructed a hollow cathode formed of aluminum foil in the shape of a cylinder; this served to contain the glow within the confines of the cathode geometry and enabled Paschen to study the structure of the helium spectrum and correlate it with Bohr's theories. Further investigations were carried out by Sawyer and Paschen [78], and by Frerichs

[79], and Takahashi [80] who investigated the mechanism of glow discharge ignition. Further work by Sawyer [81] elucidated the role of the carrier gas and metastable atoms in the mechanism of the glow discharge. Other work in the 1920s and 1930s concentrated on the use of hollow cathode lamps as a light source for analytical studies and included work by Konovalov and Frisch [82], Schuler [83], and Gollnow [84]. After World War II, McNally et al. investigated the relationship between the emission in a glow discharge and the material sputtered from the cathode into the discharge zone and used this to perform analytical determinations by measuring the emission of elements such as sulphur, fluorine and other halogens with detection limits in the μg/g range with samples weighing only a few mg [85].

In the 1950s, research on the glow discharge continued in several areas. Milestone research occurred by Birks [86] and Gromov [87] in using hollow cathode lamps as light sources in atomic absorption spectroscopy. Walsh developed the hollow cathode lamp as an emission source for atomic absorption spectroscopy in 1955 [88]. Both these developments sparked the interest in the glow discharge and specifically the hollow cathode discharge as a versatile tool for analytical spectroscopy research that continues today. Notable research into the mechanism responsible for the discharge effect was conducted by Little and Engle [89] in 1954, Crosswhite et al. [90] in 1955, Sturges and Oskam [91], and Falk [92] in 1965. Other scientists extending the capabilities of this radiation source were Eichoff, Runevskii, Maksimov, Thorton, and Torok [93, 94].

The first suggestion of using a glow discharge to obtain an atomic vapor directly from a sample for spectrochemical analysis (other than emission) was by Russell and Walsh [95], and later Russell, Walsh, and Gatehouse [96] constructed a hollow cathode device for sample sputtering and analysis by atomic absorption. It was used to determine silver in concentrations of 0.005 to 0.05 percent in copper. As successful as this device was it took the development of a new type of glow discharge for emission analysis by Grimm in 1967 to produce a renewal of interest in low pressure discharges for sample solid sample analysis [97, 98]. The Grimm discharge found a wealth of uses in emission studies for metallurgy and mineralogy and created increased interest in the glow discharge as sample sputtering device. The device immediately proved useful for the atomic absorption analysis of solution residues with work by Gandrud and Skogerboe in 1971 [99]. During the late 1970s a great deal of interest was placed on using glow discharge atomizers for atomic absorption with work by Ivanov, Gusinskii, and Esikov [100]; Yokoyama and Ikeda [101]; Bordanali and Biancifiori [102]; and Massmann [103].

The first use of a glow discharge device as a sputtering atomization source for atomic fluorescence spectroscopy was by Gough, Hannaford, and Walsh who used a demountable flat cathode sample holder in a pyrex vacuum chamber and high intensity hollow cathode lamps for excitation [104]. The elements nickel (Ni), Cr, copper (Cu), Mn, and silicon (Si) were determined with detection limits between 20 and 400 ppm. Their work continued in 1980 with the use of a nondispersive spectrometer with a similar flat cathode sample holder [105]. They obtained

detection limits approximately an order of magnitude better than comparable atomic absorption measurements. Fluorescence was used as a diagnostic method for the various processes occurring in a glow discharge by van Dijk, Smith, and Winefordner in 1982 [106]. This work also represented the first use of laser excitation of the sputtered atomic vapor produced by a glow discharge device. Here a continuous wave Ar^+ pumped tunable dye laser was used to excite the fluorescence of sodium sputtered from a demountable glow discharge tube in order to study spatial distribution of Na atoms after being sputtered off the planar cathode rod. In this study, a value for the diffusion coefficient of sodium in argon was obtained from the time-resolved fluorescence profile. Population ratios of various excited levels were observed, and it was concluded that no single excitation temperature dominated anywhere in the discharge region. Emission intensities were resolved as function of the axial position between the two electrode rods in the discharge. In 1984, Smith, Omenetto, and Winefordner used a similar planar cathode rod discharge to atomize lead from copper rods to be excited to fluoresce by a nitrogen-pumped tunable dye laser [107]. This work was the first to pulse the discharge synchronously with a pulsed laser in order to observe the fluorescence signal in the low emission background between discharge pulses. Here, two types of lead samples were determined, NIST standard copper alloy rods certified for lead concentrations between 0.4 to 128 μg/g and aqueous solutions of lead introduced on the cathode by air drying 5 μl aliquots on spectroscopically pure graphite electrodes. Detection limits were 0.1 μg/g for the copper alloy and 20 pg for the aqueous samples. The

same system was used by Patel, Smith, and Winefordner in 1985 to observe the presence of diatomic lead molecules formed in the glow discharge [108].

A demonstration of the ultimate capabilities of the glow discharge atomizer for atomic fluorescence with laser excitation was demonstrated by Smith, Womack, Omenetto, and Winefordner in 1989 by using a commercial hollow cathode lamp as an atom cell for atomic fluorescence studies of Lead [109] (see Figure 2-2). A tunable dye laser pumped by a copper vapor laser was used to excite lead atoms in the lamp whose density was controlled by controlling the current to the discharge. The current was controlled over the range of 0.001-10 mA by varying a ballast resistor in series with the lamp. The fluorescence in the lamp was observed using the pierced mirror collection system mentioned earlier. The experimental detection limit obtained here was 6000 atoms of lead in the laser probe volume within the cathode. Encouraged by this a demountable hollow cathode device for atomic fluorescence atomization was developed by Glick, Smith, and Winefordner [110]. Here aqueous solutions were dried in disposable graphite cup electrodes which were placed in a water cooled cathode holder which was fitted into a commercial vacuum chamber which served as the anode of the discharge. A xenon-chloride (XeCl) excimer pumped tunable dye laser was used to excite both lead and iridium atoms to fluoresce. This device was operated in the pulsed mode synchronously with the pulsed laser and detection limits were 500 fg for lead and 20 pg for Ir. It was this device which was the forerunner to the system used in this thesis project.

Figure 2-2. Schematic Diagram of Optical Layout of LEAFS in a Hollow Cathode Lamp with the Cu Vapor Laser. From Smith, Womack, Omenetto and Winefordner [109].

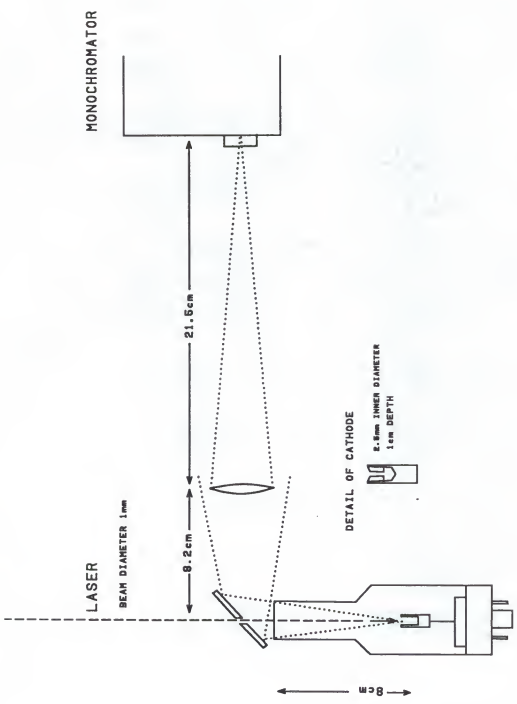
MONOCHROMATOR
LASER
BEAM DIAMETER 1mm
8.2cm
21.6cm
DETAIL OF CATHODE
2.8mm INNER DIAMETER
1cm DEPTH
8cm

CHAPTER 3
BASIC THEORY OF LASER EXCITED ATOMIC FLUORESCENCE

Theory of Single Step Atomic Fluorescence

As has been stated before, atomic fluorescence is the phenomenon that occurs when an atom emits a photon after being excited by photon absorption [1]. Therefore, the fluorescence emission event is always preceded by an absorption event with its own inherent processes and theoretical principles. These absorption transitions are based on well known quantum theory selection rules and the electronic states of the atom. Exhaustive treatments of absorption phenomena can be found in a classic monograph by L'vov [111], various chapters in Alkamade's well known monograph [112], and in a review by Piepmeier [113].

Fluorescence transitions are usually characterized into five basic categories [114]: (1) resonance fluorescence, in which the same upper and lower levels are involved in the excitation-deexcitation process; (2) direct line fluorescence, in which the upper level is only the same for the excitation-deexcitation process; (3) stepwise line fluorescence, in which different upper levels are involved; (4) sensitized fluorescence, where a donor species is excited and transfers its energy to an acceptor species either species of which then deexcites radiationally; and (5) multiphoton fluorescence, where two or more photons excite an atom through real or virtual levels with subsequent radiational deexcitation.

Several subcategories exist also. For Stokes fluorescence, the excitation energy is greater (shorter wavelength) than the fluorescence energy, while in anti-Stokes fluorescence, the excitation energy is lower (longer wavelength) than the fluorescence energy. If both the radiational excitation and deexcitation involve excited states the process is said to be excited. If the excitation process involves a collisional excitation following the radiational excitation, then it is termed thermally assisted fluorescence.

There have been several exhaustive treatments in the literature on fluorescence radiance expressions, each one having its basis on different treatments of the same phenomenon. Demtröder uses a semiclassical and quantum mechanical approach [115], Thorne uses a more general spectrophysical approach to simultaneously explain several phenomenon [116], and Omenetto and Winefordner use an approach based on rate equations [117, 118]. What follows is an overview of fluorescence equations based on the rate equation approach from a review by Winefordner [47], and a monograph by Piepmeier [119].

Several assumptions have been made in the following: (1) the atom has only two or three energy levels where listed and is not influenced by the presence of higher levels; (2) the atoms are evenly distributed in the atomizer and the atomizer has a uniform temperature with all species in thermodynamic equilibrium; (3) the light source radiation does not affect the velocity or energy distribution of the gaseous atoms; (4) the analyte atom density is low and therefore optically thin; (5) the source radiation density is spatially uniform and constant across the atomizer,

and polarization and coherence effects are negligible; and (6) the source is assumed to be quasi-continuum ($\Delta\lambda_{source} >> \Delta\lambda_{line}$).

The fluorescence radiance for a basic two level atomic (B_F) is given by

$$B_F = \left(\frac{l}{4\pi}\right) Y_{21} E_\nu(\nu_{12}) \int_0^\infty k(\nu)d\nu \tag{3.1}$$

where

l = path length in direction of detection system, m

4π = number of steradians in a sphere (fluorescence is isotropic), sr

Y_{21} = fluorescence power (quantum) efficiency, dimensionless

$E_\nu(\nu_{12})$ = spectral irradiance of exciting radiation at absorption line, ν_{12}, W m^{-2} Hz^{-1} (1 W = 1 Js^{-1})

$\int_0^\infty k(\nu)d\nu$ = integrated absorption coefficient over absorption line, m^{-1} Hz

The integrated term is given is given by

$$\int_0^\infty k(\nu)d\nu = n_1\left(\frac{h\nu_{12}}{c}\right)B_{12}\left[1 - \frac{g_1 n_2}{g_2 n_1}\right],\ m^{-1}Hz \tag{3.2}$$

where

$h\nu_{12}$ = energy of the exciting photon, J

c = speed of light, m s^{-1}

B_{12} = Einstein coefficient of induced absorption, m^3 J^{-1} s^{-1} Hz

g_1, g_2 = statistical weights of states 1 and 2, respectively, dimensionless

n_1, n_2 = concentration of states 1 and 2, respectively, m^{-3} (note that $n_1 + n_2 = n_T$, the total concentration of atoms in all states)

When using the steady state approach, one considers the excitation rate to equal the de-excitation rate; that is

$$\left(k_{12} + \frac{B_{12}E_v(\nu_{12})}{c}\right)n_1 = \left(k_{21} + A_{21} + \frac{B_{21}E_v(\nu_{12})}{c}\right)n_2 \qquad (3.3)$$

where

k_{12}, k_{21} = excitation and de-excitation non-radiational (collision) rate constants, s^{-1}

A_{21} = Einstein coefficient of spontaneous emission, s^{-1}

B_{21} = Einstein coefficient of induced emission, $m^3\ J\ s^{-1}\ Hz$

B_{12} = Einstein coefficient of induced absorption, $m^3\ J\ s^{-1}\ Hz$

n_1, n_2 = concentrations of electronic states 1 and 2, m^{-3}

c = speed of light, $m\ s^{-1}$

Based on this approach the fluorescence power (quantum) efficiency Y_{21} is given as;

$$Y_{21} = \frac{A_{21}}{A_{21} + k_{21}} \qquad (3.4)$$

One can obtain A_{21} from B_{21} and B_{12} by

$$A_{21} = \left(\frac{8\pi h\nu_{12}^3}{c^3}\right)B_{21} = \left(\frac{8\pi h\nu_{12}^3}{c^3}\right)\left(\frac{g_1}{g_2}\right)B_{12} \qquad (3.5)$$

where h is Planck's constant. Combining these expressions with equation 3.1 gives

$$B_F = \left(\frac{1}{4\pi}\right)Y_{21}E_v(\nu_{12})\left[n_1\left(\frac{h\nu_{12}}{c}\right)B_{12}\left(\frac{E_v^*(\nu_{12})}{E_v^*(\nu_{12}) + E_v(\nu_{12})}\right)\right] \qquad (3.6)$$

where

$$E_{\nu}^{*}(\nu_{12}) = \frac{cA_{21}}{B_{21}Y_{21}} \tag{3.7}$$

Some interesting conclusions can be made from the 2 level fluorescence irradiance, B_F

1) B_F is linear with n_T as long as the optical density is low.
2) If the concentration n_T is increased greatly, then B_F is not linear with n_T but is related to $\sqrt{n_T}$.
3) If a narrow line source is used for excitation then the expression for B_F is more complex. B_F is still linearly related to n_T but now the source irradiance absorbed is determined by the width and profile of the excitation line, the velocity distribution and broadening mechanisms for the absorbers.

Using the same rate equation approach one can obtain similar equations for two cases of the more realistic three level atom. One type known as a sodium (Na) type has 3 energy levels: 1, 2, 3, in ascending energy order where levels 2 and 3 are not radiation coupled. The other case has the same levels with levels 2 and 1 not radiationally coupled. This case is known as a thallium (Tl) type atom. With these 3 level atom the quantum efficiencies for the transitions are given as follows:

Na type:

$$Y_{31} = \frac{A_{31}}{(A_{31} + k_{31} + k_{32})\left(1 - \dfrac{k_{32}k_{23}}{(A_{31} + k_{31} + k_{32})(A_{21} + k_{21} + k_{23})}\right)} \tag{3.8}$$

$$Y_{21} = \frac{A_{21}}{(A_{21} + k_{21} + k_{23})\left(1 - \dfrac{k_{32}k_{23}}{(A_{32} + k_{31} + k_{32})(A_{21} + k_{21} + k_{23})}\right)}$$

Tl type:

$$Y_{31} = \frac{A_{31}}{A_{31} + A_{32} + k_{32} + k_{31}} \tag{3.9}$$

$$Y_{32} = \frac{A_{32}}{A_{31} + A_{32} + k_{32} + k_{31}}$$

Based on this, the equation for the fluorescence irradiance are as follows:

Na type atom: $$B_{\substack{F_{3-1} \\ 1-3}} = \frac{l}{4\pi} A_{31} h\nu_{31} n_T \frac{g_3}{g_1} \frac{E_\nu(\nu_{31})}{E_\nu^*(\nu_{31})} \tag{3.10}$$

Tl type atom:

$$B_{\substack{F_{3-1} \\ 1-3}} = \frac{l}{4\pi} A_{31} h\nu_{31} n_T \frac{g_3(E_\nu(\nu_{31}))}{g_1 E_\nu^*(\nu_{31})\left[1 + (g_2/g_1)\, e^{-E_{12}/kT}\right]} \tag{3.11}$$

With the use of high intensity sources one can achieve saturation. This occurs when the population of the state from which excitation occurs becomes locked to the

population of the excited state in the ratio of the statistical weights [1]. This causes the fluorescence rate to be governed by the inherent transition properties of the atom itself and not on source fluctuations and other environmental influences. This is said to occur when a fluorescence radiance occurs which is 50% of its maximum value for a particular atom and is characterized by a source irradiance called the saturation spectral irradiance $E_v^s(\nu_{i-j})$ where i and j are the transition energy levels. The attainment of the saturation spectral irradiance somewhat simplifies the fluorescence radiance equations in the following manner.

For the two level system, the saturation spectral irradiance is given as:

$$E_v^s(\nu_{12}) = E_v^*(\nu_{12})\left(\frac{g_1}{g_1 + g_2}\right) \tag{3.12}$$

and substituting n_1 in terms of n_T, B_F is given by

$$B_F = \left(\frac{l}{4\pi}\right) Y_{21} E_v(\nu_{12}) n_T \left(\frac{h\nu_{12}}{c}\right)\left[\frac{B_{12}}{1 + \dfrac{E_v(\nu_{12})}{E_v^s(\nu_{12})}}\right] \tag{3.13}$$

If $E_v(\nu_{12}) > E_v^s(\nu_{12})$ then

$$B_F = \left(\frac{l}{4\pi}\right) Y_{21} E_v^s(\nu_{12}) n_T \left(\frac{h\nu_{12}}{c}\right) B_{12} \tag{3.14}$$

or substituting for $E^s_\nu(\nu_{12})$ from equation 3.7 and 3.12

$$B_F = \left(\frac{l}{4\pi}\right) h\nu_{12} A_{12} n_T \left(\frac{g_1}{g_1 + g_2}\right) \tag{3.15}$$

This can also be extended to the two cases of the three level atom system. For these the saturation spectral irradiance is given by:

For the Na like atom:

$$E^s_\nu(\nu_{13}) = E^*_\nu(\nu_{13}) \frac{g_1}{g_3} \left(1 + \frac{g_1}{g_3} + \frac{k_{32}}{k_{23} + k_{21} + A_{21}}\right)^{-1} \tag{3.16}$$

For the Tl like atom

$$E^s_\nu(\nu_{13}) = E^*_\nu(\nu_{13}) \frac{g_1}{g_3} \left(1 + \frac{g_1}{g_3} + \frac{A_{32} + k_{32}}{k_{21}}\right)^{-1} \tag{3.17}$$

and from these, one can obtain the radiance expression under saturation conditions for several cases of each type of atom. Here the subscripts for B_F refer to the fluorescence and absorption transitions, e.g. $B_{F_{\substack{2-1\\1-3}}}$ means that the excitation is set at λ_{13} and fluorescence is measured at λ_{21}

For the Na type atom:

Saturated resonance fluorescence

$$B_{F_{\substack{3-1\\1-3}}} = \frac{l}{4\pi} A_{31} h\nu_{31} n_T \left(1 + \frac{g_1}{g_3} + \frac{k_{32}}{A_{21} + k_{21} + k_{23}}\right) \tag{3.18}$$

Saturated Stokes stepwise line fluorescence

$$B_{F_{\substack{2\to1\\1\to3}}} = \frac{l}{4\pi} A_{21} h\nu_{21} n_T \frac{g_3 k_{32} E_\nu(\nu_{31})}{g_1(A_{21} + k_{23} + k_{21}) E_\nu^*(\nu_{31})} \tag{3.19}$$

Saturated stepwise line fluorescence

$$B_{F_{\substack{2\to1\\1\to3}}} = \frac{l}{4\pi} A_{21} h\nu_{21} n_T \left[1 + \frac{A_{21} + k_{21} + k_{23}}{k_{32}} + \left(1 + \frac{g_1}{g_3}\right)\right]^{-1} \tag{3.20}$$

[Note: for the opposite cases, where excitation is at $1 \to 2$ replace all 2's by 3's and all 3's by 2's.]

For the Tl type atom:

Saturated resonance fluorescence

$$B_{F_{\substack{3\to1\\1\to3}}} = \frac{l}{4\pi} A_{31} h\nu_{31} n_T \left(1 + \frac{g_1}{g_3} + \frac{g_2}{g_3} e^{-E_{12}/kT} + \frac{A_{32} + k_{32}}{k_{21}}\right)^{-1} \tag{3.21}$$

$$B_{F_{\substack{3\to2\\1\to3}}} = \frac{l}{4\pi} A_{32} h\nu_{32} n_T \frac{g_3 E_\nu(\nu_{31})}{g_1 E_\nu^*(\nu_{31})\left[1 + (g_2/g_1) e^{-E_{12}/kT}\right]} \tag{3.22}$$

$$B_{F_{\substack{3\to2\\1\to3}}} = \frac{l}{4\pi} A_{32} h\nu_{32} n_T \left(1 + \frac{g_1}{g_3} + \frac{g_2}{g_3} e^{-E_{12}/kT} + \frac{A_{32} + k_{32}}{k_{21}}\right)^{-1} \tag{3.23}$$

Key to Symbols

l = emission (fluorescence path length), m

$h\nu_{ul}$ = energy of emission photon, J

n_u = upper (radiative) level population density, m^{-3}

n_T = total population density of *all* electronic states of same atom, m^{-3}

g_l, g_u = statistical weights of lower and upper levels, respectively

$k(\nu)$ = atomic absorption coefficient at frequency ν, m

$E_\nu(\nu_{ul})$ = source spectral irradiance at ν_{ul}, J s^{-1} m^{-2} Hz^{-1}

$E^*_\nu(\nu_{ul})$ = modified saturation spectral irradiance at ν_{ul}, J s^{-1} m^{-2} Hz^{-1}

$$= \frac{cA_{ul}}{B_{ul}Y_{ul}} = \frac{8\pi h\nu^3_{ul}}{c^2Y_{ul}}$$

B_{ul} = Einstein coefficient of induced emission, s^{-1} (J/m^3Hz^{-1})

k = pseudo-first-order radiationless rate coefficient between levels shown, s^{-1}

A = Einstein coefficient of spontaneous emission between levels shown, s^{-1}

E_{12} = energy separation between levels 1 and 2, J

k = Boltzmann constant, J K^{-1} $atom^{-1}$

T = temperature of gas, K

c = velocity of light in vacuum, m s^{-1}

Basic Theory of Lasers

All true lasers have three basic elements in common [120]: (1) an active medium which amplifies the incident electromagnetic wave; (2) an energy pump which selectively populates selected energy levels in the active medium and does so

with enough energy to achieve population inversion; and (3) an optical resonator consisting of two opposing mirrors which stores part of the induced emission concentrated within a few energy levels. Lasing action occurs when the energy pump generates a population inversion in the lasing medium. Because of this inversion, the induced emission rate exceeds the absorption rate for a transition, and an electromagnetic wave passing through this medium corresponding to the emission transition is amplified instead of attenuated. The resonator mirrors selectively feedback the radiation emitted from the excited atoms or molecules in the medium. When a certain pump threshold is reached, the feedback converts the amplifier into a laser oscillator. With the electromagnetic energy of the induced emission stored by the resonator within a few modes, the spectral energy density in these modes becomes very large.

The laser beam radiation is characterized by the following unique light source properties of directionality, high radiance, monochromaticity and coherence [121].

Directionality

Laser radiation is usually well confined to a few milliradians beam divergence because of the geometry of the resonator. The property is limited however by optical diffraction and the presence of off axis modes.

High Irradiance

This property is defined as the radiant power (W) per unit surface area (cm^2). The high irradiance of a laser is due to the confinement of the radiant power into a relatively compact and directional beam.

Monochromaticity

The laser bandwidth may be many orders of magnitude lower than the spontaneous emission bandwidth. This is a result of the higher gain of the optical amplifier at the central wavelength of the lasing medium's active transition and the wavelength selectability of the resonant cavity.

Coherence

Coherence is the orderly relationship of one part of a beam to another and can be classified as either temporal or spatial. Spatial coherence is defined by the equality of the phasing of the electromagnetic fields in the laser beam as they transverse the beam space. Temporal coherence is defined by the existence of a constant phase difference in the electromagnetic field at any given point in the beam over time.

Lasers can operate in several modes including, continuous wave (cw), pulsed, Q-switched and mode locked [1]. A continuous wave laser has an output beam that is continuous with respect to time. To achieve this, the upper level of the active transition must be longer lived than the lower level. In a pulsed laser, the output appears as a repetitive pulse train or conversely it can be operated in a single shot mode. Here, the upper lasing level must have a shorter lifetime than the lower level and the lasing action is termed self-terminating. The radiant power of a pulsed laser can be very high per pulse even if the average power is relatively low. In a Q-switched laser, the cavity is "spoiled" and oscillation is prevented until the population inversion has grown well beyond the threshold limit at which point the cavity is

switched on and a powerful giant laser pulse occurs. In mode-locking the phases of the oscillating modes are forced to be correlated or locked to each other rather than at random. This results in ultrashort pulses of high peak power. The technological aspects of obtaining these modes can be found in excellent monographs by Svelto [120], Demtroder [115], and Siegman [121]. Most spectroscopists prefer pulsed lasers because of their power, versatility, and reliability. Examples include nitrogen, excimer, Nd-YAG, and Cu-vapor lasers.

The Copper Vapor Laser

The copper vapor laser is a pulsed metal vapor laser that uses atomic copper vapor as its active lasing medium. It was developed in 1966 by Walker, Solimene, Gould, and Pilch [122] who proposed a new class of lasers known as metal vapor lasers, of which the Cu vapor was the first. Other metal vapor lasers include, Pb, gold (Au), Ca, strontium (Sr), and Mn. The first Cu-vapor lasers achieved only 20 mW of power and lifetimes of only a few hours. Recent commercial versions are capable of up to 100 W of power and lifetimes of several hundred hours. Typical applications of this laser are underwater communications and ranging, high speed photography and holography, semiconductor research, fingerprint detection, and spectroscopy [123].

The copper vapor laser produces laser oscillation in the green (510.5 nm), where efficiency is greater than 1%, and in the yellow (578.2 nm) (see Figure 3-1). The lasing action is self-terminating and therefore the laser is a pulsed laser. A general scheme for the relevant energy levels for copper is shown in Figure 3-1.

Figure 3-1. Lasing Diagram for a Cu Vapor Laser.

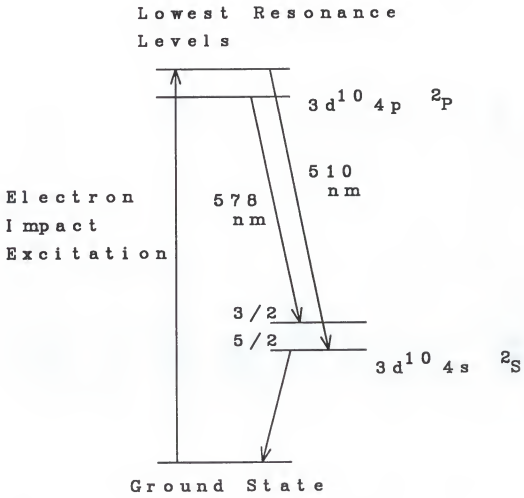
Lowest Resonance Levels
$3d^{10}\,4p\ \ ^2P$
510 nm
578 nm
Electron Impact Excitation
3/2
5/2
$3d^{10}\,4s\ \ ^2S$
Ground State

Lasing action is accomplished by thermal production of ground state copper atoms from the solid and electrical pumping of the ground state (^2S) to the lowest resonance levels (^2P). Radiational deexcitation then follows to the split metastable levels. From the metastable levels, collisional deactivation by buffer gas (Ne) collisions completes the cycle. In order for the laser to oscillate, high Cu vapor densities are needed; therefore it must be operated at a high temperature, typically 2000 K. Because of this, the laser tube is usually made of alumina and held in an insulating oven. The buffer gas flows by the end windows at around 20 to 40 torr pressure to prevent vapor deposition on the cold windows. The laser can be run at repetition rates of between 800 and 15000 Hz; an $\approx$8 kV thyratron switching voltages from a high output power supply is used to achieve the desired repetition rate (usually 6000 Hz.).

The Dye Laser

Because pump lasers are restricted to a very narrow range of wavelengths, their analytical usefulness would be very limited if it were not for their ability to pump dye lasers. A laser pumped organic dye solution will sustain lasing action over a wide wavelength range, typically 20 to 100 nm, and the use of different dyes allows lasing action from $\approx$300 to 1000 nm with different pumping methods. Dye lasers can also be pumped by flashlamp pumping, as well as pulsed and cw lasers. For the sake of brevity, only pulsed laser pumped dye lasers will be considered here. Reviews of the other types are available [124, 125].

Most pulsed laser pumped dye lasers are of the Hansch or transverse pumping design [126]. Here, the exciting laser is focused along an axis perpendicular to the dye laser axis with a cylindrical lens focused on a thin dye flow channel in the dye cell. This creates a thin line of fluorescence across the front of the dye cell as shown in Figure 3-2. Since excitation lasers are so intense during their pulse, a nearly total population inversion occurs for the dye molecules within the excitation region. This dye cell is contained within an oscillation cavity with an output coupler at one end and a diffraction grating at the other. This grating serves to tune the lasing output to a narrow bandwidth (typically 0.01 to 0.02 nm). A beam expander is placed between the dye cell and the grating to enable the beam to cover the grating and magnify the angle of diffraction leaving the grating. An etalon can be placed between the beam expander and grating if a narrower spectral bandwidth is desired. Since the oscillator cell is usually saturated, one or more amplifier cells can be added to the dye laser after the oscillator cavity with the excess pump laser power and the oscillator beam directed through it increasing the net output of the system.

Nonlinear Optics

The final technique used to obtain laser wavelengths not obtainable through pump or dye lasers is nonlinear optics. In spectroscopy, non-linear crystals are used to double or triple the frequency of the laser light incident upon them, thus providing wavelengths in the useful ultraviolet region. A full description of nonlinear optical phenomenon is beyond the scope of this dissertation but a brief discussion of the specific case of frequency doubling (second harmonic generation) may be useful.

Figure 3-2. Construction of a High Power Tunable Dye Laser.

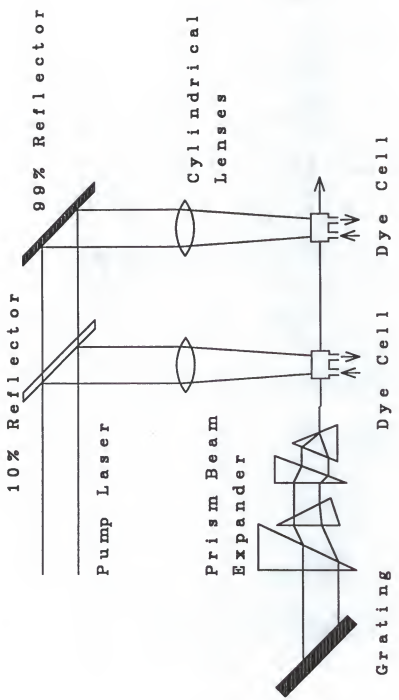
10% Reflector
99% Reflector
Pump Laser
Prism Beam Expander
Cylindrical Lenses
Grating
Dye Cell
Dye Cell

More intensive treatments of the subject can be found in a monograph by Levenson [127], and reviews by Hellwarth [128], and Druet and Taran [129].

Second harmonic lightwave generation begins when light propagates through a crystal creating an electromagnetic field within the crystal causing its electrons to oscillate. These oscillations create their own electromagnetic radiation. This effect is usually negligible but with power densities of lasers in the 10^9 W/cm^2 range (corresponding to field strengths of 10^6 V/cm) the effect begins to be noticeable in certain materials. These materials are birefringent or have two indices of refraction for the same wavelength giving rise to an ordinary and an extraordinary light ray. Frequency doubling is based upon a phenomenon called phase matching. Phase matching occurs when the incoming wave and the generated harmonic wave remain in phase. A common index of refraction is necessary for the two waves to travel the same path through the crystal and thus to achieve phase matching; this is only possible for a birefringent material. Birefringence is dependent on incidence angle, temperature and polarization, and by optimizing these one can enable the harmonic wave to be generated through the entire length of the crystal thus generating a substantial harmonic of the incident light. With lasers, the doubled light can be quite intense and coherent. Typical nonlinear crystals used in spectroscopy are potassium dihydrogen phosphate (KDP), beta-barium borate (BBO), lithium niobate, urea etc. Other nonlinear phenomena used in spectroscopy are, 3rd and 4th harmonic generation, frequency summing or mixing, Raman processes and Brillouin scattering.

CHAPTER 4
PRINCIPLES OF OPERATION AND OTHER ASPECTS OF THE GLOW DISCHARGE

Basic Glow Discharges

The term "glow discharge" is used to describe one type of electrical discharge in a gas of which there are several other types. Gaseous discharges simply refer to the flow of electric current through a gas, which requires a certain fraction of the gas particles to be ionized and an electric field to exist in the gas to accelerate charged particles and form a current [130]. Glow discharges are a steady state gas discharge as opposed to a transient discharge such as a spark. Steady state discharges can be one of three types depending on the current and voltage present. These three types are a Townsend discharge, a glow discharge, and an arc discharge (see Figure 4-1). In most cases, these discharges are maintained by a dc potential between two electrodes although one can also have discharges excited by radio frequency (rf) or microwave radiation. The Townsend discharge is a very low current discharge (nA to μA) that is not self-sustaining in that it does not produce its own ions, but requires an external source such as X-rays or UV light to produce the electrons needed for current to flow [75]. At the other end of the current range is the arc discharge which is a highly luminous discharge characterized by currents of around 1 A. It is a self-sustaining discharge producing electrons by thermionic emission from the cathode and is responsible for severe electrode erosion [131-134]. The type of discharge

Figure 4-1. Diagram Relating Different Types of Gaseous Discharges on Their Current and Voltage Characteristics. Section A Is a Townsend Discharge. Section B Is a Transition Zone. Section C Is a Glow Discharge with a "Normal" Cathode Fall. Section D Is a Glow Discharge with an "Abnormal" Cathode Fall. Section E Is an Arc Discharge.

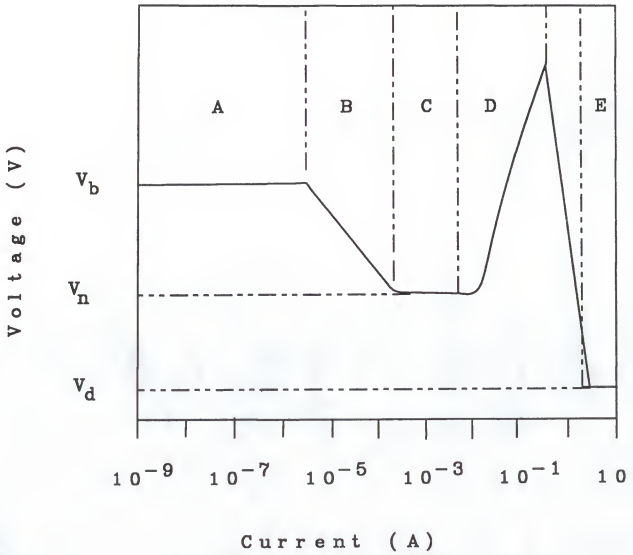
A
B
C
D
E
V_b
V_n
V_d
Voltage (V)
10^{-9}
10^{-7}
10^{-5}
10^{-3}
10^{-1}
10
Current (A)

characterized by currents in the milliampere range are known as glow discharges. These are by far the most important type analytically and will be considered in depth in the following discussion.

A glow discharge is a type of plasma, which is a partially ionized gas consisting of approximately equal numbers of positively and negatively charged species and a large number of neutral species [135]. With conventional discharges potentials of 500-1000 V are applied across planar electrodes separated by an inert gas held in a vacuum chamber at pressures of 1-10 torr. The luminous area of the discharge is characterized by a series of light and dark zones or regions (see Figure 4-2). These zones correspond to changes in several variables such as potential distribution, field strength, net space charge, negative and positive charge distribution, and negative current density [136].

Adjacent to the cathode is a dark area called the Aston dark space. This area is characterized by a negative space charge. This is caused by the presence of secondary electrons produced by Auger type energy transitions to the cathode material lattice from neutralization of the bombarding ion species by field emitted electrons just before the ion's impact with the cathode surface [137]. Primary current is carried in this region by the positive ions heading toward the cathode. At greater distances from the cathode, the electric field becomes weaker and the electrons present are more efficient excitation and ionizing agents causing electron multiplication and ionization of the discharge gas. This creates a small luminous region called the cathode layer. The next region is called the cathode (or Hittorf)

Figure 4-2. Diagram Showing Various Luminous Regions of a Glow Discharge Between Two Planer Electrodes and the Distribution of Various Other Physical Properties.

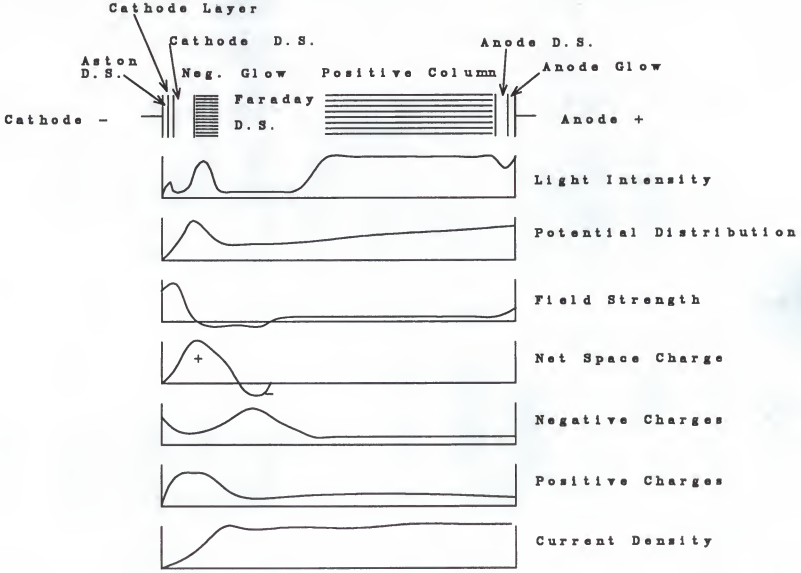
Cathode Layer
Cathode D.S.
Anode D.S.
Aston D.S.
Neg. Glow
Positive Column
Anode Glow
Faraday D.S.
Cathode -
Anode +
Light Intensity
Potential Distribution
Field Strength
+
Net Space Charge
Negative Charges
Positive Charges
Current Density

dark space. Here, only fast electrons that have not lost their energy to inelastic collisions are able to ionize atoms in this region. Because a large number of positive ions have been created in these areas near the cathode, a large positive space charge is present in the cathode dark region which produces a large potential gradient. Most of the discharge voltage drop occurs here. The voltage across the cathode dark space, from the cathode to the anode end, is called the cathode drop or cathode fall potential. At the end of the cathode dark space the positive space charge has been decreased substantially by electron multiplication and conversely the electron density has risen greatly.

The next region is a large highly luminous region called the negative glow. Here two types of electrons are accelerated through the region ionizing the discharge gas. These are fast electrons produced near the cathode which have suffered few inelastic collisions in the cathode dark space, and slow electrons created in the cathode dark space which are less energetic. The glowing color of the negative glow region is characteristic of the discharge gas, i.e., blue for argon, orange for neon, etc. The maximum brightness occurs a short distance into the negative glow from the cathode direction. As the distance from the cathode increases, the lower the energy and number of electrons present and the lower the excitation and ionization energy available. It is here at the edge of the negative glow where a region called the Faraday dark space begins.

In the Faraday dark space, the electric field again increases and pulls electrons from the negative glow accelerating them into an area called the positive column.

Here, there are equal numbers of positively and negatively charged particles giving rise to a zero net space charge and some luminosity. The anode in a glow discharge simply serves to collect electrons and as they are accelerated from the positive column, and an anode dark space occurs until the electrons acquire enough energy to ionize the gas once more and an anode glow ensues adjacent to the cathode surface. Under certain special circumstances, other regions can be observed in a glow discharge such, as the Crooke's dark space near the cathode layer, luminescent bands adjacent to the positive column, and others [75].

Glow discharges can be operated in one of two modes, the "normal" mode and the "abnormal" mode. In the normal mode the glow covers only a portion of the cathode surface, and this area is dependent on the current flowing through the discharge. Once the effective area of the cathode has been completely covered by the negative glow an abnormal glow discharge occurs. Under these conditions an increase in current flow requires a greater current density. This is only possible with a larger cathode fall, and thus the voltage must increase. It is preferable to operate in the abnormal mode since homogeneous sampling of the whole cathode surface occurs [130].

Hollow Cathode Discharges

The differences in the characteristics of a planar glow discharge as described above and those of the hollow cathode discharge are solely related to its geometry and how that alters the discharge performance. An easy way to visualize these differences and their cause is to consider a glow discharge with two parallel cathodes

brought close enough together that the negative glow regions of the two merge into one. This proximity of one cathode surface to the other serves to trap the electron density within the walls of the hollow cathode. This is made possible because the mean free path of electrons in a noble gas at glow discharge pressures are large enough to allow some of them to reach the opposite wall of the cathode [130]. The positive space charge is then almost reduced to zero, the current intensity increases and the cathode fall diminishes. This current density is several orders of magnitude higher than that obtained with a normal planar glow discharge and subsequently a large increase in excitation and ionization occurs. Since the current density inside the cathode is much higher inside the cathode than outside, the discharge is confined to the interior surfaces of the cathode.

Because of electron confinement in the hollow cathode discharge, only the characteristic discharge regions from the cathode layers to the negative glow are present inside the hollow cathode. Measurements in the negative glow of an argon hollow cathode discharge's electron energies by Howorka and Pahl [138] using a Lanqmuir probe reveal the presence of three different groups of electrons based on their kinetic energy. The very fast electrons have energies of 100 eV and over resulting from the strong acceleration of the cathode fall. Fast electrons occurred from direct ionization and slow electrons generated in the negative glow plasma make up the other two groups. The fast electrons have energies of around 3 eV while the slow electrons have energies of less than 0.5 eV. The electron energies do not change along the axis of the cathode but electron density increases towards the

open end of the cathode. Electron number densities vary with discharge parameters but usually fall in the range of 10^{11} to 10^{13} cm^{-3} for currents below 1 A.

Sample Sputtering in the Hollow Cathode Discharge

One of the most interesting phenomenon that occurs in the glow discharge is the formation of an atomic vapor composed of atoms from the cathode material. The process by which this takes place is called sputtering [75]. Sputtering is a physical process where atoms are ejected from the cathode surface. This occurs when the positive fill gas ions and metastable atoms impact the cathode surface after being accelerated through the cathode potential fall from the negative glow region. The energetic atom that strikes the cathode surface is either backscattered (a low probability event, estimated at 10^{-3}), or penetrates the solid cathode material and dissipates its energy to the surface atoms [139]. Secondary electron emission caused by the impact uses up the potential energy of the impacting ion while its kinetic energy and momentum are transferred to the cathode atom lattice through collisions. A collision cascade occurs in the immediate area with the initial impact lasting around 10^{-12} s [140]. Atoms at or near the surface can acquire enough energy from these collisions to overcome their surface binding energies and be ejected from the surface. The escape depth or sampling depth depends on the characteristics of the collision cascade but generally the sampling depth amounts to one quarter of the penetration depth, generally 3-5 Å.

Extraction of atoms from the cathode surface requires that the impacting ion have energy levels above a certain threshold level that depends on the fill gas and

the target (cathode) material. The surface binding energy of the target can be approximated by the heat of sublimation of the material. A good rule is to consider the kinetic energy required for sputtering to be at least four times the heat of sublimation of the target material [130]. This usually lies between 15 and 35 eV. Above this threshold energy, the amount of sputtered material rises first exponentially, reaching a flat plateau, and then decreasing with increasing energy. Because of the surface binding energy, different elements do not have identical sputter atom yields. Typically yields increase with atomic numbers within any one period of the periodic chart, moreover, it is interesting to note that these yields rarely differ by more than a factor of ten. If target materials contain more than one element then preferential sputtering does take place altering the surface concentration of different elements from that of the bulk concentration throughout the sample. In this fashion, the overall sputtering rate is equal to that of the component having the slowest rate [141].

The fill gas and surface roughness also contribute to the sputtering rate. Obviously, the more massive the impacting atom is the higher the sputtering efficiency. One can easily see then why neon is a much better fill gas than helium as far as sputtering is concerned for most samples; however, the most efficient sputtering occurs when the fill gas atoms and the target atoms have nearly the same mass. The roughness of the target surface also contributes to the sputter yield because a sputtered atom may not be able to clear the surface features and then may become reattached somewhere else.

The target temperature seems to play little role in the sputtering process until the temperature approaches values where evaporation becomes superimposed on sputtering, thereby increasing the apparent sputter yield. This seems to occur when the cathode surface reaches a temperature about 250 K below the target metals melting point.

Quantitative relationships revealing sputtering yields and rates based on other known quantities are usually valid only for specific systems and thus no general equation for sputtering yield has yet been developed. Caroli proposed the following equation based on empirical studies for hollow cathodes [94];

$$Q = CL^2th^{-1}F^{-1}p^{-1} \tag{4.1}$$

where

Q = The current dependent sputter rate (reduced sputter rate) in $\mu g\ A^{-1}\ s^{-1}$

C = Empirical constant related to the fill gas and cathode material (unitless)

L = Applied power in W

t = Sputtering time in s

h = Hollow cathode depth in mm

F = Hollow cathode frontal area in mm^2

p = Gas pressure in torr

This equation is a simplified way of relating the experimentally determined constant C to the sputter yield than to create a theoretical model. More realistic treatments

have determined that the sputter yield is proportional to the discharge current raised to a factor of between 2.5 and 3.5 depending on the fill gas pressure (the lower the pressure the higher the exponential factor) [109,142-147].

Once the target atoms are released from the surface, several things can happen to them, including: excitation, ionization, recombination with the electrode, combination with other species or surfaces, or simple diffusion away from the cathode. Cathode bombardment results in the removal of a large number of neutral target atoms as well as a few positive and negative target ions. It has been shown that the positive ions make up less than 1% of the total number of sputtered species [148]. This is because these positive ions are returned to the cathode by the prevailing electrical field in the cathode fall region. The field also serves to accelerate secondary electrons and negative target ions away from the cathode. Sputtered neutral atoms, consisting of mostly ground state species, are ejected from the cathode with energies of around 5-15 eV. These atoms rapidly lose their initial energy as a result of the many collisions possible with atoms of the discharge gas. In a 1 torr discharge, this may cause as much as 95% of the sputtered atoms to be redeposited on the cathode surface [149]. Sputtered atoms that escape backdiffusion and redeposition enter the negative glow region of the discharge where they can be excited or ionized by several modes.

Ionization of neutral cathode atoms in the glow discharge is mainly caused by either electron impact or Penning ionization [149-155] but can also be caused by many other secondary ionization mechanisms including symmetric and nonsymmetric

charge transfer, associative and dissociative charge transfer, and photoionization [156,157].

Table 4-1. Primary Ionization Mechanisms

Electron Impact	Penning Ionization
$M^o + e^- = M^+ + 2e^-$	$M^o + A_m^* = M^+ + A^o + e^-$
(M^o = sputtered neutral)	(A_m^* = metastable fill gas atom)

Electron impact ionization of the sputtered neutral species probably contributes the most in the cathode fall region and in the region of low field intensity between the cathode fall region and the negative glow region. Between 0.1 and 1% of the sputtered neutral population may be expected to be ionized by electron impact [130].

When a ground state atom collides with an excited atom whose energy is greater than the first ionization potential of the neutral species, that species can undergo excitation. When the originally excited atom is at a metastable energy level from which radiative transition to the ground state is forbidden, this process is known as Penning ionization. Because of the long lifetimes of the metastable atoms, they seem to have a large role in the ionization of sputtered neutrals. Argon, for example, has metastable energy states of 11.55 eV and 11.72 eV, values exceeding the first ionization potentials of nearly all elements. These metastable species are produced very efficiently by electron collisional events in the discharge with densities

of between 10^{10} to 10^{11} cm^{-3} reported [148]. The cross sections for Penning ionization do not seem to vary greatly from element to element and it is responsible for up to 5% ionization of the sputtered neutral species. Penning ionization may take on an even larger role in the ionization of neutral sputtered atoms in pulsed glow discharges.

CHAPTER 5
EXPERIMENTAL

The overall layout of the experimental system can be found in Figure 5-1. The complete system can be divided into four groups; (1) the laser excitation system, (2) the glow discharge atomization system, (3) the fluorescence collection, signal detection and data processing system, (4) and the sample preparation system. Each one of these subsystems will be examined in detail.

The Copper Vapor Pumped Dye Laser System

The copper vapor laser used in these experiments was a Metalaser Technologies/Cooper Lasersonics model CVL251 copper vapor laser available from Laser Photonics, Orlando, FL. The laser was equipped with stable resonators and operated at a repetition rate of 6000 Hz although this could be varied from 4000 to 12000 Hz by the external triggering system. This triggering system consisted of a function generator and digital counter (model FG501A and DC503A, Tektronix, Inc., Beaverton, OH) which triggered a pulse generator (model 802, Wavetek, Inc., San Diego, CA) used to shape the trigger pulse to the specifications of the laser manufacturer. This laser has an average power of 20-22 W and a peak power of 140 kW in a 25 ns pulse with an input power of 7.8 kV at 6000 Hz.

Figure 5-1. Schematic Diagram Showing the Experimental Layout of the LEAFS Glow Discharge System.

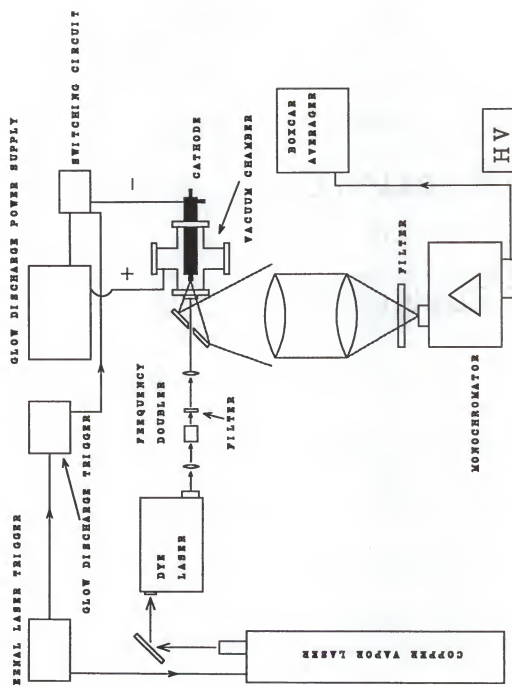
EXTERNAL LASER TRIGGER
GLOW DISCHARGE TRIGGER
GLOW DISCHARGE POWER SUPPLY
SWITCHING CIRCUIT
COPPER VAPOR LASER
DYE LASER
FREQUENCY DOUBLER
FILTER
CATHODE
VACUUM CHAMBER
BOXCAR AVERAGER
FILTER
MONOCHROMATOR
PMT
HV
+
-

This laser was used to pump a dye laser (Molectron DLII, Laser Photonics) flowing organic dyes through flowing dye cells. The dye pumping system used a laboratory constructed 2 L dye reservoir with chilled water cooling. This cooling of the dye extended its useful life by several hours by reducing thermal decomposition by the pump laser. The dye system used the high speed dye pump and filter supplied with the laser from the manufacturer.

The fundamental output from the dye laser is restricted to the visible wavelength region by the pumping wavelengths. Because most nonresonance excitation lines for the elements studied in the glow discharge are in the ultraviolet region, frequency doubling of the fundamental output was required. This was done using a variety of nonlinear crystals (Interactive Radiation Corp., Northvale, NJ). The visible radiation from the dye laser was focused to a point just before the doubling crystals by a 150 mm focal length lens, noting that it is important not to focus the beam inside the crystal in order to prevent thermal damage to the crystal. The proper polarization of the fundamental beam with relation to the doubling crystal is important for maximum efficiency and this was ensured with the intracavity polarizer provided with the dye laser. Color filters were used (Corion Corp., Holliston, MA) to separate the UV light output from the visible light passing through the doubling crystal. Average energies obtained in the UV were between 200 and 600 nJ per pulse in a 20 ns pulse with a spectral bandwidth of 0.02 nm.

The ultraviolet light was then focused into the atomizer system by a 1 cm diameter, 150 mm focal length quartz spherical lens. The UV beam was not tightly

focused in the sampling volume of the atomizer but had a beam diameter of around 1 mm. This was done to increase the probe volume somewhat and was possible because the laser output was well above the saturation irradiance for all the elements studied.

The Glow Discharge Atomizer

The glow discharge system can be subdivided into two parts; the hollow cathode and vacuum chamber, and the power supply and pulsing system.

Hollow Cathode and Vacuum Chamber

The hollow cathode of the glow discharge is actually a commercial disposable graphite electrode cup (Model HPHD-2041D and HPHD-4001D, Spectrographic Services, Sussex, NJ). These electrodes are slip-fitted into a machined tubular brass cathode holder. This cathode holder is water cooled through interior cooling passages and is insulated from the discharge by a fitted quartz sleeve surrounding it completely except for the aperture where the electrode is fitted. All exposed portions of the graphite electrode except the interior of the cup itself are insulated from the discharge by ceramic sleeves fitted over the electrode. The entire cathode assembly is fitted into the vacuum chamber and sealed with an o-ring fitting at the rear of the cathode holder. A electrical connection on one of the water inlet tubes serves to connect the cathode to the power supply. A schematic of the cathode holder assembly can be found in Figure 5-2.

Figure 5-2. Schematic Diagram Showing the Water Cooled Cathode Holder and Disposable Graphite Electrode.

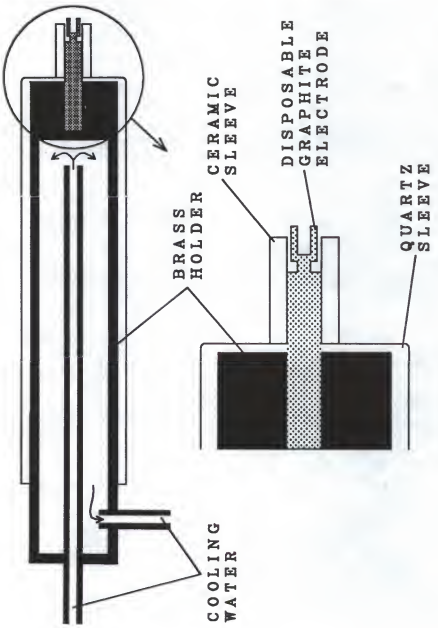
BRASS HOLDER
CERAMIC SLEEVE
DISPOSABLE GRAPHITE ELECTRODE
QUARTZ SLEEVE
COOLING WATER

The vacuum chamber itself is a commercial six way, 2.25 in flange, vacuum cross (Huntington Labs). The chamber is electrically grounded and serves as the anode of the discharge. One flange serves as the vacuum connection with the cathode holder and is designated the rear flange. The flange directly opposite the cathode holder is fitted with a quartz window to admit the frequency doubled laser beam and to allow viewing of the fluorescence. The bottom port serves as a mounting point to attach the vacuum chamber to a custom x-y-z translation stage used to align the glow discharge with the dye laser. The left side flange serves as a connection to the vacuum pump used for the system and the right flange is connected to the vacuum monitoring manometer (Model Baratron 221A, MKS Systems, Burlington, MA). The argon fill gas inlet was located near the manometer port and was a 1/2 in Cajon type fitting. A gate valve on the top flange allowed venting of the chamber to atmosphere as necessary.

The gas handling system consisted of a high flow rotary vacuum pump (model 1400, Duo-Seal, Inc., Skokie, IL) used to maintain vacuum in the chamber, and two precision needle valves and a manifold to control the argon flow into the chamber. The supply manifold had an independent pressure gauge so that the pressure to the needle valves could be controlled independently from the argon tank pressure.

The Power Supply and Pulsing System

The power supply for the glow discharge was a 3 kV high output power supply (Model 803-330, Hipotronics, Inc., Brewster, NY). It was equipped with a multiple range voltage readout and a multiple range current readout, both analog meters.

The power supply was voltage monitored and maintained the set voltage by changing the current to compensate for changes in resistance. It was also equipped with selectable ground polarity that was maintained in the negative position.

The glow discharge was pulsed synchronously with the laser system by using the same external triggering system used for the copper vapor laser to trigger the pulsing system of the discharge. This system consisted of another Wavetek model 802 pulse generator used to shape and delay the discharge pulse after being triggered by the laser pulsing system. The actual circuit used to pulse the discharge was the same as previously used by Glick, et al. [110] and is depicted in Figure 5-3. The only modifications were to use a larger main ballast resistor that was forced air cooled to enable the use of higher voltages and repetition rates. Using the Wavetek pulse generator, the discharge pulse could be varied from 0 to 100 μs in duration and delayed up to 75 μs after the laser pulse. In actual operation, the laser triggers the next pulse of the discharge but excites the atoms created in the previous laser pulse. The laser-discharge pulse timing was set up and checked by monitoring the emission and laser scatter signal from the detector with a digital oscilloscope (Model 2040A, Tektronix Corp.) (see Figure 5-4). If desired, the discharge could be operated in a non-pulsing continuous mode by switching off the Wavetek pulse generator which disabled the pulsing circuit.

The actual pulsing voltage to the discharge could be switched off or on by a high voltage switch placed directly in the high voltage supply to the discharge. This was done to enable the setting of all discharge parameters including voltage before

Figure 5-3. Schematic Showing the Glow Discharge Pulsing Circuit.

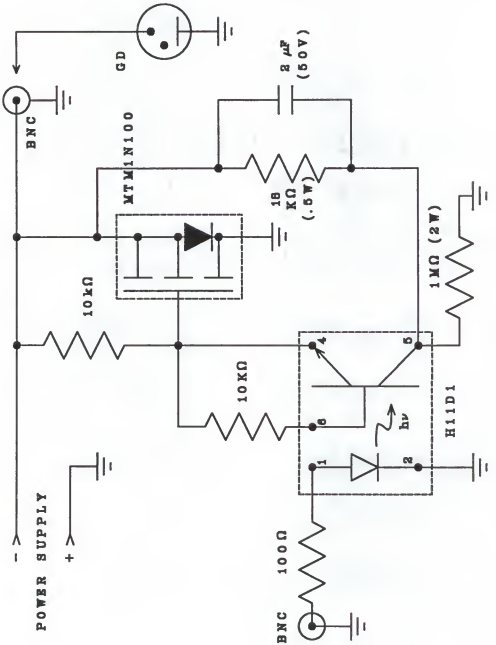
GD
BNC
2 μF (50V)
MTM1N100
18 KΩ (.5W)
10 kΩ
1MΩ (2W)
10KΩ
H11D1
hν
BNC 100Ω
POWER SUPPLY
-
+

Figure 5-4. Diagram Illustrating the Laser Pulse Causing a Fluorescence Pulse 100 μs After the Glow Discharge Pulse. Taken From Oscilloscope Monitoring PMT Detector.

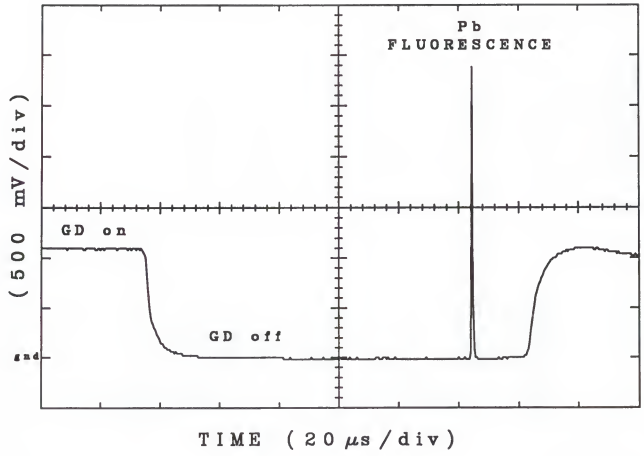
Pb
FLUORESCENCE
GD on
GD off
(500 mV / div)
TIME (20 μs / div)

igniting the discharge. This enhanced the reproducibility of the routine sample analysis experiments.

The Fluorescence Collection, Signal Detection and Processing System

Fluorescence Collection Optics

The fluorescent light was collected from the hollow cathode through the viewing window on the vacuum chamber by a 45° pierced plane mirror. The mirror had a 3 mm diameter center aperture that allowed the frequency doubled output to pass through it. The image was directed by the mirror to a 10 cm diameter spherical plano convex quartz lens (20 cm focal length) which collimated the light and directed it to a second identical lens which focused a 1 to 1 image of the fluorescence on the 1.25 mm slit of a 0.25 meter monochromator (Model Minimate, f/4, 10 nm spectral bandpass, Spex Industries, Inc., Edison, NJ). Scatter from the laser excitation light was reduced to the monochromator by a variety of coated glass and solution filters (to be discussed in chapter seven) placed before the slit.

Signal Detection and Processing

The detector used to detect the fluorescent light selected by the monochromator was a fast response photomultiplier tube (model R955, Hammamatsu Corp., Bridgewater, NJ) with an anode to cathode voltage of -1000 volts supplied by a high voltage power supply (Model EU42A, Heath, Acton, MA). The anode current pulse was terminated into a 1000 ohm resistor. The resulting voltage pulse was 200 ns FWHM.

The voltage pulse was sent to low noise preamplifier (Model 4131, Evans Assoc., Berkeley, CA) and then to a boxcar integrator (Model SR250, Stanford Research Systems, Palo Alto, CA) which was set to average 3000 pulses with a gate width of 100 ns and a 70 ns delay. The effective instrumental bandwidth for all measurements was 1 Hz.

The data from the boxcar was sent to a microcomputer (Model 286, PC's Unlimited, Austin, TX) for processing and storage using the Stanford software supplied with the boxcar integrator. The date is transferred by an analog to digital computer interface (Model SR245, Stanford Research Systems). This interface, however, is unable to transfer the data faster than 1.2 kHz. Because the interface is triggered by the busy out signal from the boxcar, which is at the laser repetition rate of 6 kHz, a simple divider circuit must be used to divide the trigger signal to the interface by a factor of ten. At 600 Hz, the interface transfers all the data points taken because it contains a buffer memory which accumulates untransferred data points until they can be sent.

Sample Preparation and Analysis Procedure

Sample Preparation

Sample preparation began by pretreating the sample electrode (hollow cathode sample holder). This was done by placing the electrode between the electrodes of an electrothermal atomizer (ETA) work head (Model CRA90, Varian Instrument Division, Palo Alto, CA) and activating the ETA's programmable power supply in the "max temp" mode. This heated the electrode to 2500 K for 10 to 30 s.

The electrode is left in the furnace work head and after it has cooled the desired amount of sample (usually 2 to 40 μL) is injected into the cathode cup. After injection, the power supply is activated after having been programmed to undergo a 60 to 180 s drying cycle at 103° C. This is done to dry the sample thoroughly. Argon is passed over the electrodes during all heating cycles to lessen thermal decomposition of the electrodes. After being allowed to cool under flowing argon, the sample holder is fitted to the cathode holder and the ceramic sleeve then fitted over it. The entire assembly is then placed in the vacuum chamber for analysis of the sample.

Analysis Procedure

For analysis of a routine sample, the vacuum chamber is pumped down to the lowest pressure attainable (usually around 0.1 torr) for 1 min after insertion of the loaded cathode holder. Argon gas is then allowed to flow through the chamber for 30 s and the pressure in the vacuum chamber brought up to the desired value. The power supply to the discharge is set to the desired voltage but with the external high voltage switch in the off position. The laser, having been previously tuned to the desired wavelength, is then allowed to enter the discharge chamber and the high voltage to the discharge switched on. After allowing 10 s for the discharge to stabilize, the data acquisition is begun.

Preparation of Solutions and Cleaning of Glassware

Stock solutions of 1000 μg/ml for all the elements studied were either prepared from reagent grade chemicals in deionized water as described in the

literature [1,126] or the stock solutions from commercial sources were used. The working standard solutions were prepared by serial dilution from the stock solutions on an as needed basis.

All volumetric flasks used were soaked in concentrated nitric acid for 24 hours, then rinsed with first distilled and then deionized water. All volumetric pipets used for the serial dilutions of the standards were soaked for 24 hours in a detergent solution, then rinsed with first concentrated nitric acid, distilled water, and finally deionized water immediately before their use.

CHAPTER 6
OPTIMIZATION OF GLOW DISCHARGE PARAMETERS

To obtain the highest fluorescence sensitivity from the system, several operational parameters must be experimentally optimized. This optimization must be done to ensure that the glow discharge atomizer is providing the maximum number of atoms from the sample in a form that can be excited by the incoming photons from the laser system. These parameters include optimizing the vacuum chamber pressure, cathode material and dimensions, injected sample volume, the discharge voltage, and finally, the timing of the glow discharge pulse with the laser pulse to obtain the maximum fluorescence signal. All of the parameter investigations were carried out using lead as the element of analysis. The nonresonance fluorescence transition for lead was used with the laser tuned to an excitation wavelength of 283.31 nm and the monochromator was set to look at the fluorescence at 405.7 nm. The dye used in the dye laser was rhodamine 590 at a concentration of 4×10^{-4} M in methanol (HPLC grade, Fisher Scientific). The doubling crystal used was KDP (model R6G, Interactive Radiation Corp.) with a colored glass filter (Model UG-5, Corion Corp.) used to pass the UV light while blocking the visible light from the dye laser. A sharp cut glass filter (Model LG-350, Corion Corp.) was used to block the laser scatter from the monochromator in all lead determinations.

Signal Dependence on Vacuum Chamber Pressure

The optimization of the vacuum chamber pressure for maximum fluorescence was first experimentally determined for a solid sample. Here a solid sample of 5 mg Pb shavings (reagent grade, Fisher Scientific, Fair Lawn, NJ) was placed in a pretreated graphite electrode and then inserted in the glow discharge chamber for analysis. The discharge voltage was held at a constant 1000 V, and the chamber pressure varied using the gas control needle valves from 0.5 torr to 13 torr in a flowing gas environment. In this way a plot of fluorescence signal versus vacuum chamber pressure was obtained. Since a sufficient quantity of lead remained in the hollow cathode electrode to ensure reproducibility, each point on the fluorescence signal versus vacuum chamber pressure plot represents the same lead sample left in the electrode sample holder.

The vacuum chamber pressure signal optimization was also determined for aqueous samples. In this experiment, individual 30 μL samples of 2 ppm aqueous lead are used for each point on the signal versus pressure curve. Again the voltage was a constant 1000 V for each sample, and the fluorescence signal was determined for samples with chamber pressures ranging from 0.5 torr to 13 torr.

Both of these measurements were done with the discharge operating in the flowing mode. Argon gas was continuously flowing through the discharge chamber at 1.1 L/min. The glow discharge could also be operated in a static gas flow mode. Static gas flow conditions were obtained by simply closing a gate valve on the vacuum side of the glow discharge chamber after vacuum below 0.2 torr had been reached.

The fill gas control valves were then opened momentarily to allow the argon fill gas to bleed into the chamber until the desired pressure is reached. The vacuum chamber is capable of maintaining a constant pressure for several minutes as long as the discharge is off. Once the discharge ignited, the pressure in the chamber would rise at a rate of about 3.6 torr/min.

A comparison was made between the flowing system and the static gas system by analyzing two 30 μL aqueous 2 ppm lead samples. Each sample was analyzed at 1000 V and 10 torr chamber pressure. The only difference in the two samples was that one sample was analyzed under flowing gas conditions and the other under static gas flow conditions.

The results of the optimum pressure measurement experiments can be found in Figure 6-1. The signal versus pressure curves show very similar behavior for both the solid and aqueous samples dried on the electrode. Both exhibit a sharp peak from 1 to 2 torr which falls off sharply and plateaus from 4 to 8 torr. The signal then increases from 8 to 13 torr and levels off at higher pressures. The difference in intensity between the solid and aqueous samples is simply due to the differing amounts of lead on the electrode. The general trends followed by the signal pressure curves can possibly be explained by noting the generally equivalent maxima of the peaks at 1-2 torr and again at 8-15 torr. From chapter 4, we know that the lead atoms generated by the glow discharge and responsible for the fluorescence signal are directly related to the number of argon ions generated in the negative glow region. These ions are accelerated toward the cathode surface impacting as either

Figure 6-1. Plot Showing Dependence of Fluorescence Signal to Vacuum Chamber Pressure for Both Solid Lead and 2 ppm Aqueous Lead Dried on the Cathode.

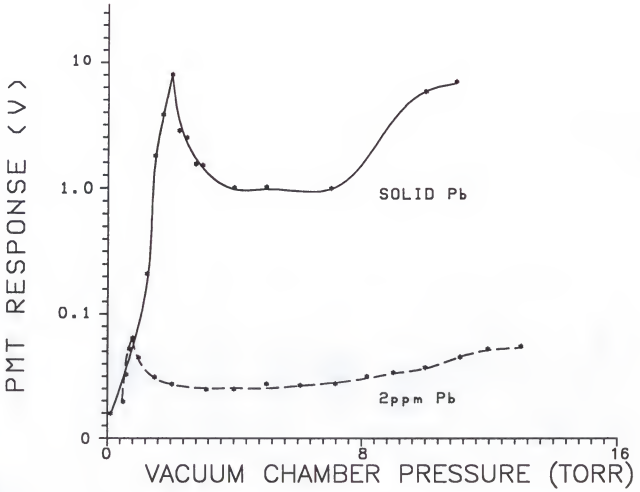
PMT RESPONSE (V)
10
1.0
0.1
0
SOLID Pb
2ppm Pb
0
8
16
VACUUM CHAMBER PRESSURE (TORR)

the ion or as a metastable atom created from the ion in the cathode dark space. Since the production of these ions is related to the number of electrons present and this is kept constant by the constant current, the increasing pressure must cause an increase the argon atom density. Once the argon atom density is roughly equal to the electron density, the number of ions formed in the negative glow region does not increase with increasing pressure and only the ratio of argon atoms to ions formed increases. It is possible that the first peak is caused by the rapid increase of argon ions formed with increasing pressure until the population of ions and electrons equilibrates. This equilibration then slowly creates an increasing plateau from 2 to 13 torr and up. The dip in the plateau from 2 to 8 torr may be caused by the recombination of the lead atoms with the cathode surface. As pressure increases, the mean free path of the sputtered lead atoms decreases so that recombination with the electrode surface becomes more likely. The competition between these two processes may contribute to the shape of these curves.

As far as determining the optimum pressure for fluorescence measurement, it appears to make no difference whether one operates at the low pressure maximum or the high pressure maximum. The signal to noise in both regions is comparable. For most measurements, high pressure maximum was used to circumvent any substantial signal deviations caused by small pressure fluctuations at the lower pressure maximum.

The comparison of the flowing system to the static gas system gave mixed results. When the determination was performed on two similar samples under both

conditions, the static gas system gave a 10 fold increase in the signal over the flowing gas system. Unfortunately, the noise in the signal increased appreciably more. Thus the signal to noise of the flowing gas system was better than that of the static gas system. The signal increase in the static gas system was invariably caused by the increased residence time of the sample atoms in the probe volume. The noise increase is thought to be caused by the fluctuations in pressure in the vacuum chamber after the static gas discharge was ignited. These fluctuations gave rise to instabilities in the discharge itself which caused noise in the signal. Because of these considerations, the flowing gas system was found to be more favorable for fluorescence measurements.

Signal Dependence on Injected Sample Volume and Cathode Cup Diameter

To determine the effect of injected sample volume on the fluorescence signal, a series of determinations were done on 2 ppm aqueous lead samples of sample volumes varying from 2 to 50 μL. All other discharge parameters were kept constant with the discharge voltage at 1000 V and the vacuum chamber pressure at 10 torr. An experiment was also undertaken to determine any differences caused by cathode cup diameters. Here similar 30 μL samples of 2 ppm aqueous lead are measured in two different size cathode cups. One cathode cup was 0.32 cm interior diameter and 0.5 cm deep, while the other cathode cup was 0.44 cm interior diameter and 0.16 cm deep. All samples were again measured under the same discharge parameters of 1000 V potential and 10 torr pressure.

The results of the fluorescence signal versus injected sample volume can be seen in Figure 6-2. While possibly linear at very low sample volumes, the curve shows a decreasing dependence of the signal due to increasing sample volume until 40 μL where any further increase in sample volume causes no increase in the fluorescence signal. Because the sample atomization is caused by surface sputtering, this behavior is to be expected. Increasing sample volume increases the surface coverage of the cathode cup and thus increases the sputtering yield. Once the active surface has been covered with the analyte, the fluorescence dependence on the addition of more analyte is decreased. Even though the technique appears to be markedly nonlinear, linear calibration curves can be obtained if one maintains the same sample volume throughout a determination. Another effect possibly contributing to this behavior is the absorption of the analyte into the porous graphite cup material. While this is a well-known phenomenon [130], the extent it plays in the signal versus sample size is not known, but it is expected to be substantial.

In determining the effects of two different cup sizes, the signal to noise ratio is similar for both cup sizes. The larger cup, however, had more favorable ignition characteristics (see Figure 6-3) which gave lower noise during sample measurements. This was a result of the better fitting of the ceramic insulator sleeve to the exterior of the larger cup thereby insulating it better. This ensured that the discharge did not ignite on the exterior of the cup.

Figure 6-2. Plot Showing Dependence of Fluorescence Signal on Sample Volume of 2 ppm Lead Dried in the Cathode.

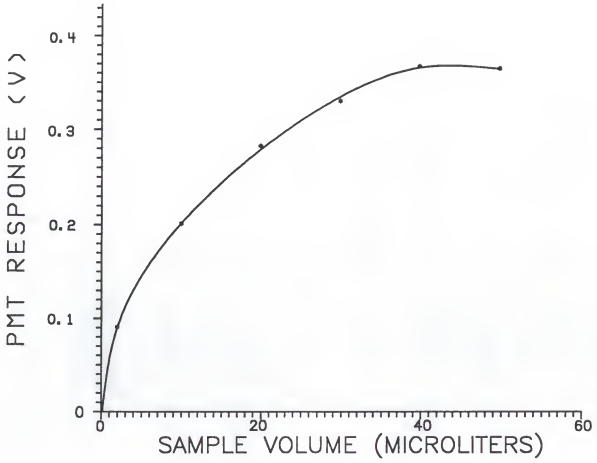
PMT RESPONSE (V)
0.4
0.3
0.2
0.1
0
0
20
40
60
SAMPLE VOLUME (MICROLITERS)

Figure 6-3. Diagram Showing Ignition Characteristics for the Two Different Size Disposable Graphite Electrodes Used.

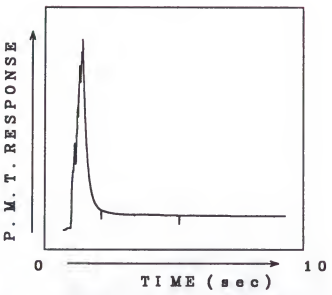

LARGE DIA. CATHODE

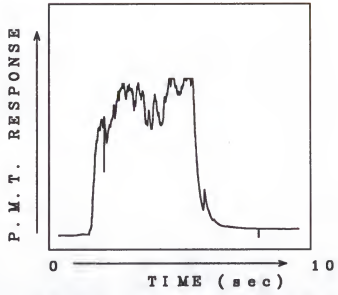

SMALL DIA. CATHODE

Signal Dependence on Discharge Voltage and Laser-Glow Discharge Pulse Timing

The dependence of the fluorescence on the voltage applied across the discharge was investigated for both solid lead and an aqueous lead salt dried on the cathode. For the solid sample determination, a 1 mg sample of solid lead shavings (Reagent grade, Fisher Scientific) was placed in a pretreated electrode and then into the glow discharge. The chamber pressure was maintained at a constant 2 torr and the voltages ranging from 280 to 1600 V were applied to the same sample. A similar experiment was performed on individual aqueous 2 ppm lead samples dried on the cathode. The vacuum chamber pressure was held constant at 2 torr and voltages ranging from 280 to 1600 V were applied. A major difference in the two experiments was that in the interest of reproducibility a new aqueous sample was used for each point on the aqueous fluorescence signal verses voltage curve.

Up to this point all measurements of the fluorescence in the pulsed glow discharge were carried out with the laser pulse probing approximately the same temporal domain between discharge pulses. In other words, the laser pulse (and thus the fluorescence pulse) was always timed to occur between halfway and two thirds of the way through the dark period between discharge pulses, or about 35 μs after the discharge pulse was switched off. This time was chosen because it allowed sufficient time for the glow discharge emission to fall to zero and was based on common sense qualitative examination of the emission signal from the glow discharge.

An interdependence of the signal-voltage response on the laser-glow discharge pulse synchronization was discovered due to the results of the solid sample fluorescence signal verses applied voltage experiment. The curve exhibited a sharp peak rising from the ignition voltage to 480 V, and then sharply declining again to a plateau at 760 V that is around half of the peak value. The signal then remained at this plateau for the remainder of the voltage range. This phenomenon was eventually thought to be caused by quenching of the analyte fluorescence by ion formation; as the voltage increased, the energy in the discharge environment became sufficient to ionize lead atoms that would otherwise fluoresce. The expected collisional energy range in the glow discharge of 5 to 15 eV [130] would be adequate to overcome the ionization potential of lead which is 7.5 eV.

This theory was first tested by a relatively simple experiment. A more easily ionizable element, 1000 μg/ml sodium (Na), was added to a solid lead sample and the fluorescence signal verses discharge voltage experiment was repeated. If ionization was responsible for the fluorescence quenching, the addition of sodium should decrease the effect. The presence of the sodium seemed to have no affect on the shape of the curve (see Figure 6-4); unfortunately, the concentration of the sodium might not have been sufficient to cause a significant perturbation. To further investigate this effect, the laser delay time with respect to the discharge pulse was decreased (see Figure 6-5). The cathode environment should contain a higher energy distribution of species closer to the discharge pulse which would enhance the ionization effect. A signal-voltage curve was obtained for an identical solid lead

Figure 6-4. Plot Showing Dependence of Fluorescence Signal on the Addition of 1000 ppm Aqueous Sodium to a Solid Sample of Lead.

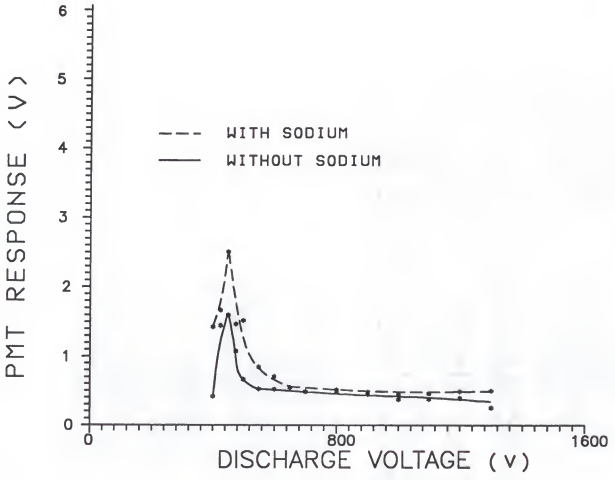
PMT RESPONSE (V)
6
5
4
3
2
1
0
WITH SODIUM
WITHOUT SODIUM
0
800
1600
DISCHARGE VOLTAGE (V)

Figure 6-5. Plot Showing the Dependence of the Fluorescence Signal of a Solid Lead Sample on Discharge Voltage for Two Different Laser-Glow Discharge Pulse Synchronizations. Curve A Represents the Laser Firing 35 μs After the Glow Discharge Pulse and Curve B Represents the Laser Firing 15 μs after the glow Discharge Pulse.

PMT RESPONSE (V)
5
4
3
2
1
0
0
800
1600
DISCHARGE VOLTAGE (V)
A
B

sample with the excitation pulse 15 μs after the glow discharge emission reached zero. The 15 μs delay curve exhibited completely different behavior than the conventional 35 μs delay curve implying a more complicated process is taking place.

After the discharge is extinguished, the gas phase environment changed rapidly over time. Immediately upon shut down the emission fell to zero within 5 μs, followed by a rapid decrease in the energy distribution and population of electrons in the discharge; however, the population of metastable argon atoms and argon ions should remain relatively constant for several milliseconds [14]. Although specific transport and excitation mechanisms for the analyte atom population are not known, it can be theorized that the analyte number density decreases rapidly as the result of several processes. These include recombination with the electrode surface, formation of metal compounds, ionization of the analyte, and evacuation of the analyte by gas flow (in the flowing gas environment). This decrease in analyte atom density makes the larger fluorescence peak for the 35 μs curve even more surprising. It is possible that the major differences between the 15 μs and 35 μs curves are the analyte atom number density, and the electron energy distribution and electron number density population. The mechanism by which these processes contribute to the curve shapes is not clear; however, the variation of discharge current with discharge voltage was investigated and found to be linear. It is interesting to note that the signal to noise for both the 15 μs and 35 μs curves was virtually identical.

Because routine analysis with the pulsed glow discharge involves aqueous samples dried on the surface of the cathode, a more intensive study of the

interdependence between fluorescence signal, discharge voltage, and laser-glow discharge pulse timing was undertaken. The first investigation involved determining the signal dependence on the discharge voltage with the laser firing 35 μs after the discharge pulse. Each point on the signal-voltage curve corresponds to a fresh aqueous lead sample (30 μL, 2.0 μg/mL) and data taken 10 s after the discharge ignition over a voltage range of 280 to 1500 V. The pressure in the discharge was maintained at a constant two torr. The aqueous sample data presents two fluorescence plateaus (see Figure 6-6). The signal levels off at an applied voltage of $\approx$400 V. The signal then remains constant to $\approx$1100 V at which point it appears to rise to another plateau which remains constant for the rest of the voltage range.

To further investigate the effect of the timing parameter on aqueous signal-voltage curves, similar experiments were performed on 20 μL, 2 μg/ml aqueous lead samples dried on the electrode for timing parameters of 16 μs, 54 μs, and 75 μs at a constant chamber pressure of two torr. An identical experiment with the same concentration of aqueous lead and the same timing parameters for a constant chamber pressure of 10 torr was performed also.

These results can be found in Figure 6-7 and 6-8. The 16 μs curve at 2 torr behaves like the previous 35 μs, 2 torr curve, with the fluorescence graduallyincreasing from 450 V to a moderately broad peak at $\approx$800 V. The other two timing parameter curves exhibit different behavior, As the timing delay between the glow discharge pulse increases, the fluorescence signal maximum shifts to lower

Figure 6-6. Plot Showing the Dependence of the Fluorescence Signal on Discharge Voltage for a 2 ppm Aqueous Lead Sample Dried on the Cathode with the Laser Firing 35 μs after the Glow Discharge Pulse.

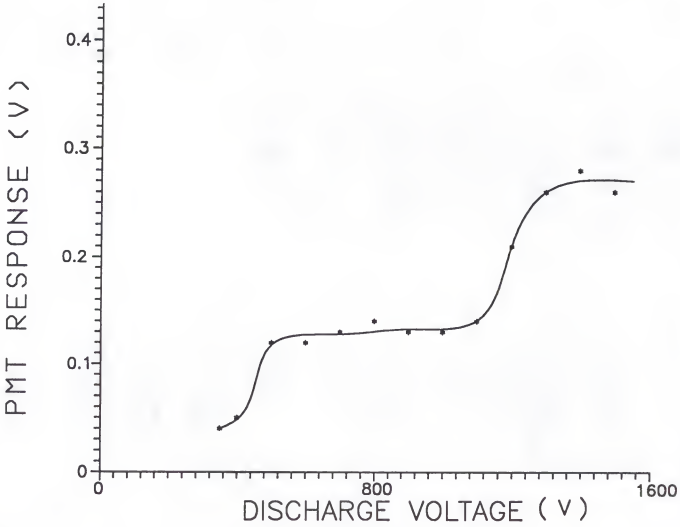
PMT RESPONSE (V)
0.4
0.3
0.2
0.1
0
0
800
1600
DISCHARGE VOLTAGE (V)

Figure 6-7. Plot Showing the Dependence of the Fluorescence Signal on Discharge Voltage for 2 ppm Aqueous Lead Dried on the Cathode With Three Different Laser-Glow Discharge Pulse Synchronizations at a Pressure of 2 torr. Curve A Represents the Laser Firing 16 μs After the Glow Discharge Pulse. Curve B Represents the Laser Firing 54 μs After the Glow Discharge Pulse. Curve C Represents the Laser Firing 75 μs After the Glow Discharge Pulse.

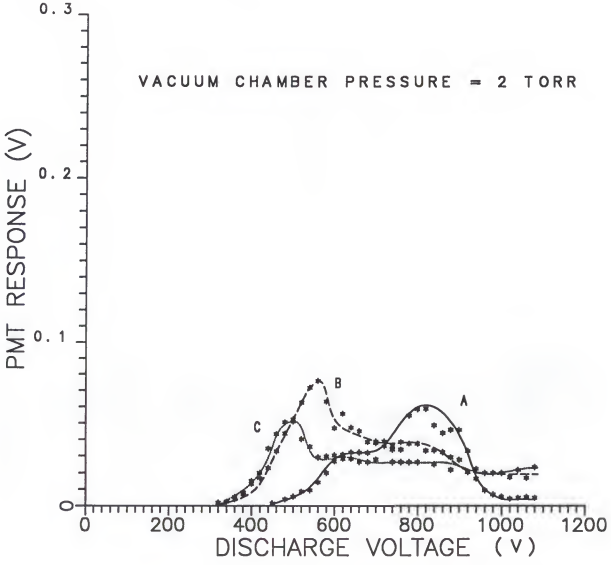
VACUUM CHAMBER PRESSURE = 2 TORR
PMT RESPONSE (V)
0.3
0.2
0.1
0
A
B
C
0
200
400
600
800
1000
1200
DISCHARGE VOLTAGE (V)

Figure 6-8. Plot Showing the Dependence of the Fluorescence Signal on Discharge Voltage for a 2 ppm Aqueous Lead Sample Dried on the Cathode With Three Different Laser-Glow Discharge Pulse Synchronizations at a Pressure of 10 torr. Curve A Represents the Laser Firing 16 μs After the Glow Discharge Pulse. Curve B Represents the Laser Firing 54 μs After the Glow Discharge Pulse. Curve C Represents the Laser Firing 75 μs After the Discharge Pulse.

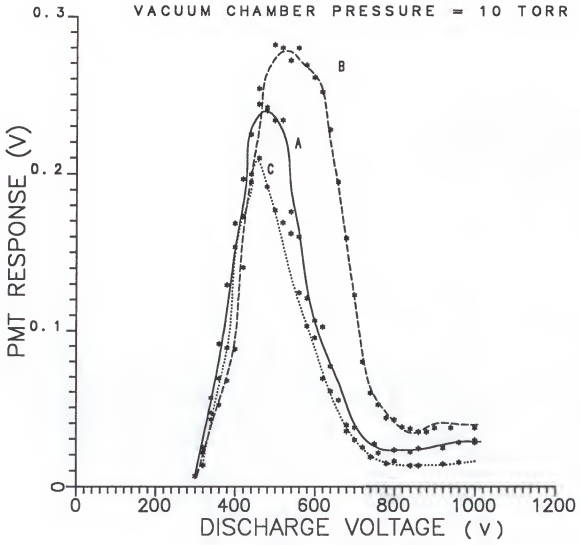
VACUUM CHAMBER PRESSURE = 10 TORR
PMT RESPONSE (V)
0.3
0.2
0.1
0
A
B
C
0
200
400
600
800
1000
1200
DISCHARGE VOLTAGE (V)

voltages, the 54 μs signal peak being at 540 V and the 75 μs peak occurring at 480 V. Both of the latter peaks gradually declined after their peaks over the remainder of the voltage range investigated.

The repetition of the experiment at the higher chamber pressure of 10 torr produced similar peak profiles for the 54 μs and 75 μs curves with the signal peaks for each at approximately the same voltage. Notice that the increase in chamber pressure from 2 to 10 torr resulted in a peak signal increase of a factor of 5. The 16 μs curve at 10 torr exhibited completely different response than its 2 torr counterpart. Instead of being shifted to higher voltages, the signal maximum was more closely related to the 75 μs signal peak. The reason for this is unknown. In all cases, the fluorescence signal was strongest for the 54 μs peak when using the aqueous samples dried on the electrode.

There are differences between the solid and dried aqueous lead samples in the glow discharge system. The drying of an aqueous sample in a graphite cup adds complication to the sampling process. In contrast to the solid sample, some analyte in an aqueous sample penetrates the porous graphite, being lost to analysis, even though a larger surface area of the cathode is covered. Aqueous samples also introduce SO_3 or NO_2 from the acids used in some sample preparations. Furthermore, it has been shown that no matter how much drying is undertaken, one cannot totally remove water from the electrode due to the porosity of the graphite.

The formation of H_3O^+ in glow discharges has been well documented [130] and this could account for some fluorescence quenching due to collisional or other processes. All of these differences may contribute to the contrasting shapes of the signal-voltage curves for the solid and aqueous samples.

CHAPTER 7
RESULTS AND DISCUSSION

Experimental Determinations of Elements

The best determination of an analytical methods usefulness is the determination of its sensitivity and range of linearity for several elements. To determine the analytical usefulness of the glow discharge as a sample atomizer for laser excited atomic fluorescence spectrometry with copper vapor pumped dye laser, the detection power of the system for the determination of several elements was investigated. These elements were lead, iridium, gallium, iron, and cobalt. All of these determinations were performed on pure aqueous solutions of the analyte dried onto the surface of the graphite electrode. To illustrate the ability of the system to analyze real samples, lead was also determined at two different concentrations in an NIST standard estuarine river sediment. For a detailed description of the general analytical procedure, see chapter 5 of this work. Any specific experimental procedures unique to a specific elements determination will be listed in this portion of the text.

The Determination of Lead

Because the element lead was used in the initial evaluation of this technique, it was the first element of which the figures of merit were determined with this

technique. Lead is an ideal element for atomic fluorescence determination because of its convenient Stokes direct-line nonresonance fluorescence transition with the convenient excitation wavelength of 283.31 nm and a fluorescence wavelength of 405.7 nm (see Figure 7-1). This large wavelength difference allows easy discrimination of the fluorescence radiation from the excitation source scatter by both sharp cut glass filters placed before the monochromator slit and by the monochromator grating itself. Because of this, lead is quoted as having some of the best detection limits in laser excited atomic fluorescence spectrometry [70, 109].

For the lead determination rhodamine 590 (Laser Grade, Eastman Kodak Co., Rochester, NY) at a concentration of 4×10^{-4}M in HPLC grade methanol was used in the dye laser to obtain visible radiation at 566.62 nm. To obtain the ultraviolet radiation at 283.31 nm needed to excite the lead fluorescence a potassium dihydrogen phosphate nonlinear optical doubling crystal (KDP-R6G, Interactive Radiation Corp.) was used to frequency double the visible radiation. A colored glass filter (Model UG-5, Corion Corp.) was used to pass the doubled ultraviolet light and block the visible fundamental beam. The fluorescence was monitored by the monochromator at 405.7 nm with 1.25 mm slit widths. Since laser scatter from several sources such as the fluorescence collection mirror, the viewing window on the glow discharge vacuum chamber and the rear surface of the hollow cathode discharge cup is prohibitive, some type of filter is needed to discriminate against the laser scatter and not the fluorescence. In the case of lead, a sharp cutoff, glass filter (model LG350, Corion Corp.) can be used with success because of the large energy (wavelength)

Figure 7-1. Partial Grotrian Diagram for Lead.

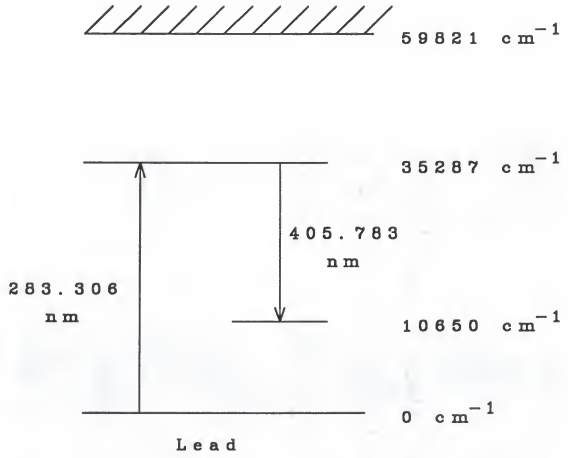
59821 cm^{-1}
35287 cm^{-1}
405.783 nm
283.306 nm
10650 cm^{-1}
0 cm^{-1}
Lead

difference in the excitation and fluorescence wavelengths. This filter is placed immediately in front of the entrance slit to the monochromator and passes better than 80% of the fluorescent light while blocking over 99% of the excitation scatter.

The standard 1000 μg/ml stock lead solution was made from carefully weighed solid lead sulfate (Reagent grade, Fisher scientific) dissolved in 5% sulfuric acid solution. Standard solutions ranging from 10 ppb to 100 ppm were made from this solution by successive dilution. The volume of solution injected into the hollow cathode was a constant 10 μL and was injected using an Eppendorf pipette with disposable pipette tips. The injected solutions were dried on the graphite electrode for 90 s at 100 °C with the programmable electrothermal atomizer power supply and work head. The calibration curve for the lead solutions was generated by measuring the lead standard solutions in the glow discharge at 1000 V across the discharge and a chamber pressure of 10 torr under flowing conditions. The laser was timed to fire 35 μs after the previous glow discharge pulse.

After the lead calibration curve had been obtained, a determination of two different lead concentrations in NIST standard reference material estuarine river sediment was performed. The river sediment was first carefully dried and weighed to constant weight on an analytical balance. The weighed material was then quantitatively transferred to a volumetric flask where it was first dissolved in a warm 10% nitric acid solution and then diluted to volume with deionized water. It was then successively diluted to obtain two solutions; one containing 570 ppb and the other containing 874 ppb lead. Four 10 μL aliquots of each of these solutions was

then analyzed in the glow discharge under the conditions listed above. The response of these solutions was compared to the previously obtained lead calibration curve.

The lead calibration curve can be seen in Figure 7-2 and is linear over four orders of magnitude and has an experimental absolute limit of detection of 15 fg base on the slope of the analytical curve, the blank noise, and a confidence factor of three. A measurement of the true blank signal for lead was impossible to obtain because of contamination of the electrodes, solutions, and apparatus by environmental lead. Because of this, the lead blank signal was obtained by detuning the laser slightly from the lead excitation wavelength, the so-called off line method. This did not change the characteristics of the background fluorescence caused by scattered laser radiation. The determination of lead in the estuarine river sediment resulted in an average of 872 ppm for the solution containing 874 ppm and an average of 563 ppm for the solution containing 570 ppm lead. The four measurements on the 874 ppm solution has a relative standard deviation of 2.5% from the calculated value and the four measurements for the 570 ppm solution had a relative standard deviation of 2.8%.

The Determination of Iridium

The element iridium was the next element of interest. For this determination an excitation wavelength of 285.0 was required. Since this is very close to the lead excitation wavelength, the same dye and doubling crystal were used to obtain the excitation wavelength for iridium. The Stokes non-resonance direct line fluorescence

Figure 7-2. Analytical Calibration Curve for Lead.

PMT response (mV)
Absolute Mass of Pb (pg)

for iridium occurs at 357.4 nm and the same sharp cut glass filter as in the lead determination was used to block the laser scatter from the entrance slit to the monochromator.

The standard solutions used to generate the iridium calibration curve were made from successive dilutions of a commercial stock solution of 1000 μg/ml iridium in 10% hydrochloric acid (Custom standard, Inorganic Ventures, Inc., Tom's River, NJ) and ranged in concentration from 100 ppb to 100 ppm. Again 10 μl samples were injected into the cathode and dried using a drying cycle of 100 °C for 90 s in the ETA. As with the lead determination, the glow discharge vacuum chamber was maintained at 10 torr and a potential of 1000 V was applied to the discharge with the laser firing 35 μs after the discharge pulse.

The results of the iridium determination can be seen in Figure 7-3. The experimental absolute limit of detection obtained from this calibration curve is 2 pg based on the slope of the calibration curve, the blank noise, and a confidence factor of three. Iridium posed no contamination problem as did lead so the blank was determined with the laser tuned to the iridium excitation wavelength.

The Determination of Gallium

The nonresonance Stokes direct line fluorescence transition for gallium places the excitation wavelength at 287.40 nm and the fluorescence wavelength at 294.40 nm. Again the same dye and doubling crystal can be used to obtain the excitation wavelength. The same colored glass filter is used after the doubling crystal to block the visible beam and allow the UV to pass. Unfortunately in this case the excitation

Figure 7-3. Analytical Calibration Curve for Iridium.

PMT response (mV)
Absolute Mass Ir (pg)

and fluorescence wavelengths are not separated enough to use a sharp cut glass filter to block the laser scatter from the monochromator. Instead a sharp cut solution filter of chlorobenzene (Certified grade, Fisher Scientific) was used with a path length of 3 cm. This provides an absorbance at the excitation wavelength of 1.000 and absorbance at the fluorescence wavelength of 0.060 (see Figure 7-4).

Standard gallium solutions were serially diluted from a commercial 1000 μg/mL stock solution of gallium in 10% hydrochloric acid (Custom Standard, Inorganic Ventures). Again 10 μL samples were dried at 100 °C for 90 s on the graphite electrode. In this measurement the vacuum chamber pressure was 10 torr, the voltage across the discharge held at 600 V, and the laser timed to fire 54 μs after the glow discharge pulse. This change in operating parameters was based on new experimental data (see chapter 6).

This measurement gave an absolute experimental detection limit for gallium of 900 pg, and the calibration curve was linear over three orders of magnitude. The detection limit was based on the slope of the analytical curve, the blank noise, and a confidence factor of three. The blank noise was again determined with the laser tuned to the gallium excitation wavelength. The dye used in this experiment was not very efficient at the required wavelength and the doubled output from the dye laser was correspondingly weak, estimated to be less than 50 Nj/pulse.

The Determination of Cobalt

The non-resonance Stokes fluorescence for Co occurs with excitation radiation at a wavelength of 304.40 nm and fluorescence at 340.5 nm. To achieve this

Figure 7-4. Absorption Spectra for Chlorobenzene Solution Optical Filter.

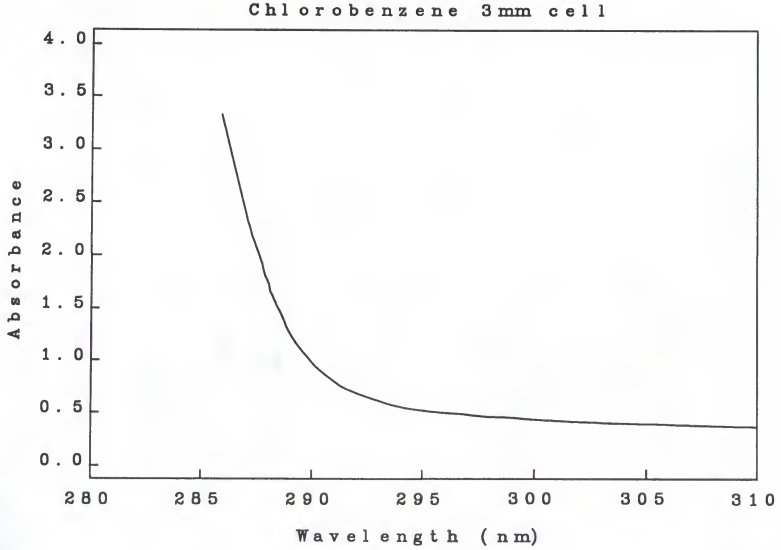
Chlorobenzene 3mm cell
4.0
3.5
3.0
2.5
2.0
1.5
1.0
0.5
0.0
Absorbance
280
285
290
295
300
305
310
Wavelength (nm)

wavelength the dye used in the dye laser was changed to kiton red 620 (Exciton Corp, Dayton Ohio) at a concentration of 1 x 10^{-3}M in methanol (HPLC grade, Fisher Scientific) to provide a fundamental output from the dye laser of 608.80 nm. This was then frequency doubled with a potassium dihydrogen phosphate nonlinear optical crystal (model KDP-B, Interactive Radiation Corp.) to obtain the UV output of 304.40 nm. Again a UG-5 colored glass filter is used to block the visible fundamental beam and pass the UV. As was the case with gallium, the energy difference of the excitation radiation and the fluorescence radiation is close enough to preclude the use of sharp-cut glass filters and to require solution filters to block the laser scatter from the monochromator. In the case of cobalt, the best solution filter to use was found to be 1, 2, 4, trichlorobenzene with a one cm path length. This provided an absorbance of 1.25 at 304.4 nm and an absorbance of 0.050 at 340.40 nm.

The standard cobalt solutions were serially diluted from a commercial 1000 μg/mL cobalt in 2% nitric acid solution (Custom Standard, Inorganic Ventures). As before 10 μL samples were injected into the graphite electrodes and dried at 100 °C for 90 s. As with gallium, the discharge voltage was 600 V, the vacuum chamber pressure was 10 torr, and the laser set to fire 54 μs after the discharge pulse.

The cobalt calibration curve was linear over four orders of magnitude and gave an experimental absolute detection limit for cobalt of 40 pg based on the slope of the

analytical curve, the blank noise, and a confidence factor of three. The blank noise was determined with the laser tuned to the cobalt excitation wavelength

The Determination of Iron

The nonresonance Stokes direct line fluorescence transition for iron is at an excitation wavelength of 296.70 nm and the fluorescence is at a wavelength of 373.5 nm. This excitation wavelength required a mixture of two dyes in the dye laser. A mixture of rhodamine 590 (3×10^{-3}M) and kiton red 620 (conc. 9×10^{-4}M) in HPLC grade methanol was used to obtain a fundamental output from the dye laser of 593.40 nm which was then frequency doubled to 296.70 nm by the same doubling crystal as used with cobalt. The same colored glass filter was used to block the visible light from the dye laser and pass the UV. With iron, an inorganic solution filter of 0.2 M potassium nitrate (KNO_3) in deionized water with a 2 cm path length was used to block the laser scatter from the monochromator. This filter provided a absorbance of 0.01 at 373.5 nm and an absorbance of 5 at 296.7 nm.

The standard iron solutions were serially diluted from a commercial stock solution of 1000 μg/mL iron in 2% nitric acid solution (Custom Standard, Inorganic Ventures.). Again 10 μL samples of each standard solution was injected onto the graphite electrode and dried for 90 s at 100 °C. The glow discharge was operated at 600 V, a vacuum chamber pressure of 10 torr, and the laser timed to fire 54 μs after the discharge pulse.

The iron calibration curve was linear over four orders of magnitude and gave an absolute experimental detection limit of 120 pg based on the slope of the

analytical curve, the blank noise, and a confidence level of three. The blank noise was determined with the laser tuned to the excitation wavelength of iron.

Theoretical Detection Limits

Calculated theoretical detection limits for laser based analytical spectrometry systems are possible and there are several treatments dealing with these calculations. An excellent overview on the subject can be found in a monograph by Stevenson and Winefordner [158]. Alkemade derived a statistical expression for calculating the detection limit that was based on fluctuations inherent in the signal itself. This is known as the "intrinsic" detection limit, which is the minimum number of atoms detectable in the probe volume [159] and is given by:

$$(N_p)_m = \frac{k^2}{\epsilon_d R_p} \tag{7.1}$$

where k is the statistical confidence factor (usually 3), R_p is the number of repeated probings and ϵ_d is the detection efficiency (number of photons detected per atom per laser pulse). The detection efficiency can be expressed as:

$$\epsilon_d = [1 - \exp(-\eta_s A_{um} T)](\Omega_F/4\pi)\eta_t \eta_{PMT} \tag{7.2}$$

The parameters for this equation can be found in Table 7-1 for a calculation of this systems theoretical detection limit for lead, which is a well characterized determination.

Table 7-1. Definitions and Parameters for Equation 7.2

Parameter	Definition	Value (this exp.)
R_p	number of laser probings	6000
η_s	saturation parameter	0.75
A_{um}	spontaneous transition probability, s^{-1}	0.9×10^{8}
T	laser pulse width, s	2×10^{-8}
Ω_F	solid angle of fluorescence collection, sr	1.1×10^{-2}
η_t	optical transmission efficiency	0.5
η_{pmt}	quantum efficiency of PMT	0.2
G	gain for PMT	10^{7}
e	charge on the electron	1.6×10^{-19}
R_L	PMT load resistance, Ω	1000
Δt	pulse width at load resistor, s	2.0×10^{-7}
T_s	lifetime of sputtered atoms, s	10^{-3}

The saturation parameter is given by the following equation:

$$\eta_s = \left(\frac{g_u}{g_u + g_l}\right)\left(\frac{I_\lambda}{I_\lambda + I_\lambda^s}\right) \tag{7.3}$$

where g_u and g_l are the upper and lower level statistical weights (3 and 1 respectively), I_λ is the spectral irradiance of the laser (J s^{-1} m^{-1} nm^{-1}) and I_λ^s is the saturation spectral irradiance for the excitation transition (J s^{-1} m^{-1} nm^{-1}). Neither of these parameters is actually known. However, since experimental proof of saturation of the lead transition exists (see Figure 7-5) the saturation parameter will have a value of 0.75. The value of the transition probability for the 405.7 lead transition is from Lotrian et al. [160]. On the basis of equation 7.2 and the values listed in Table 7-1, the detection efficiency (ϵd) for this system for the lead fluorescence is 2.59 x 10^{-4}.

The detection efficiency can be used to estimate the voltage pulse obtained at the PMT load resistor per atom per probing in the laser beam by the following equation:

$$\Delta V = e_d G e (R_L / \Delta t) \tag{7.4}$$

where the parameters are defined in Table 7-1. When these values are used in this equation a voltage pulse of 2.08 x 10^{-6} volts per pulse-atom is calculated.

When used with equation 7.1 the detection efficiency can be used to calculate the intrinsic detection limit. Using the calculated detection efficiency and parameters listed in Table 7-1, the intrinsic detection limit for lead (minimum number of atoms detectable in the probe volume) with this system is calculated to be 6 atoms. This is the theoretical detection limit as defined by the noise inherent in the analytical signal. A more realistic theoretical detection limit is the calculation of the intrinsic detection limit rate in the sample which includes the residence time of the atoms

Figure 7-5. Plot showing Dependence of the Fluorescence Signal for Solid Lead on the Laser Pulse Energy. This Plot Illustrates Optical Saturation of the Lead Fluorescence.

Fluorescence Intensity (V)
10
1
0.1
0.01
0.001
0.1
1
10
100
1000
Laser pulse energy, nJ

produced by the atomizer in the probe volume (T_s), the atomization efficiency of the system (ϵ_a), the temporal probing efficiency (ϵ_t) and the spatial probing efficiency (ϵ_s):

$$\left(\dot{N}_a\right)_m = \frac{k^2}{\epsilon_d R_p T_s \epsilon_a \epsilon_t \epsilon_s} \tag{7.5}$$

where other parameters are defined in Table 7-1. The analyte residence time (T_s) is estimated to be at least 1 ms because fluorescence could be measured up to 1 ms after the glow discharge had been extinguished. Using the best case of atomization, temporal probing and spatial probing efficiencies to be one, a value of 5.8×10^3 atoms per second was obtained. With an instrumental time constant of 1 s, this corresponds to an intrinsic detection limit in the sample for this system of 2 ag. The experimental detection limit for lead is estimated to be 10^8 atoms, based on the 15 fg experimental limit of detection, the atomization time for 90% of the lead and the time constant of the boxcar averager.

There can be many sources for the deviation of the experimental results from those calculated theoretically. Obviously the atomization efficiency, the temporal probing efficiency and the spatial probing efficiency are less than one in the experimental system. This alone can give rise to orders of magnitude differences in the experimental and theoretical detection limits. The other parameters are sufficiently well known as to maintain the uncertainty in the calculation below 50%.

Determination of the Limiting Noises of the System

The sources of the blank noise in a system that limits its sensitivity can come from many sources such as inherent noise in each part of the system (PMTs, boxcars, laser scatter etc.). An analysis of these noises was undertaken to determine the contribution of each to the total blank noise. This was done by isolating different system and removing their contribution to the blank noise. In this manner, the noise contribution of each source can be elucidated. The analysis was performed using lead as the analyte of interest so the laser and monochromator were tuned to the lead transitions of 283.31 nm and 405.7 nm respectively. The results can be found in Table 7-2.

The limiting noises were measured by sampling the filtered boxcar output for 10 s using the data acquisition software for the boxcar. The instrumental bandwidth was 1 Hz. For the purposes of calculation, the standard deviation of this data was taken to be representative of the RMS noise fluctuations. By examining the data one can ascertain that the largest noise sources were the laser scatter and the background emission; either light scattered at the laser wavelength or broadband background fluorescence caused by the laser scatter striking mirrors, lens, holders, etc., or emission from the negative glow.

Table 7-2. Limiting Noise Analysis

Limiting noise source	RMS value (μV)	LOD (fg)
laser scatter + background emission + PMT + boxcar + RFI	68	15
background emission + PMT + boxcar + RFI	60	13
laser scatter + PMT + boxcar + RFI	48	11
PMT + boxcar + RFI	4.5	1.0
PMT + boxcar	1.9	0.42
boxcar	0.7	0.02

CHAPTER 8
CONCLUSIONS AND FINAL COMMENTS

This work has demonstrated that the pulsed hollow cathode discharge is a viable alternative as an atomizer for ultra-trace analysis using laser excited atomic fluorescence spectroscopy. It provides detection limits in the femtogram to picogram range and has demonstrated an ability to analyze lead in estuarine river sediment and thus indicate it may be successful for real samples without extensive sample pretreatment. Table 8-1 compares the results of this work to similar results from other studies.

It can be seen from this table that the glow discharge does not give a detection power as good as the graphite furnace atomizer. This is because of its much lower sample atomization efficiency. It is hoped however, that the advantages of the glow discharge make it more attractive for certain real samples with matrix interferences in the graphite furnace.

The comparison of the experimental detection limits with the calculated theoretical detection limits indicate that improvement can still be made on the system to improve its sensitivity. Foremost among these is the use of pyrolitically coated graphite as the construction material for the cathode. This would lessen analyte loss absorption into the graphite matrix and enable much better atomization of the sample and possibly even re-use of the electrodes. Also with the coated graphite, smaller sample sizes could be used improving the absolute detection limit.

Other coating methods for the graphite could be attempted also to improve its impermeability also such as polystyrene and thallium iodide.

Table 8-1. Comparison of Results

Element	LOD (this work)	Literature LOD
Pb	15 fg	500 fg [110] 80 ag [70]
Ir	2 pg	20 pg [110] 0.02 pg [161]
Ga	900 pg	2 pg [70]
Co	40 pg	0.2 pg [66]
Fe	120 pg	500 fg [70]

Note: The first literature detection limit for Pb and Ir were obtained in a similar pulsed glow discharge with excimer pumped dye laser excitation. The other detection limits are in graphite furnace atomizers with various pulsed dye lasers as excitation sources including N_2, Nd-Yag, excimer and copper vapor pumped dye lasers.

Other improvements to the system would center around improving the detection efficiency through increasing the probing rate through the use of higher repetition rate or even CW lasers. Fluorescence could also be measured only in the ultraviolet region with a solar blind photomultiplier tube. Double resonance

(stepwise) excitation could be used to provide a wider range of available transitions in the UV region and improve the selectivity of the method.

This investigation into the use of a pulsed glow discharge as an atomizer for laser excited atomic fluorescence has raised questions about the many processes that occur in a glow discharge that affect the sample atoms availability for fluorescence, especially those processes that are a direct or indirect result of pulsing the discharge. It is hoped that interest will be stimulated in this area to better understand and characterize the sputtering process and enhance the glow discharge's suitability as an atomizer device.

REFERENCES

1. J.D. Ingle, Jr., and S.R. Crouch, *Spectrochemical Methods*. Prentice Hall, Englewood Cliffs, New Jersey (1988).

2. H.J. Graft and W.L. Reynolds, *Solid State Techn.* 141, 443 (1985).

3. M.S. Leleaux, *At. Spectrosc.* 8, 71 (1987).

4. R. Zeskova, C. Achenbach, H.R. Shulten, and R. Roll, *Toxicol. Lett.* 19, 225 (1983).

5. J.P. Franke and R.A. Coengracht de Zeeuew, *Arch. Toxicol.* 40, 134 (1975).

6. J. Lacke, *Anal. Chim. Acta* 113, 3 (1980).

7. W. Goody, E.I. Hamilton, and T.R. Williams, *Brain* 98, 65 (1975).

8. V.S. Letokhov, *Laser Photoionization Spectroscopy*. Academic Press, Orlando, Florida (1987).

9. G.S. Hurst and M.G. Payne, *Principles and Applications of Resonance Ionization Spectroscopy*. Hilge, Bristol (1988).

10. N. Omenetto, B.W. Smith, and J.D. Winefordner, *Spectrochim. Acta* 43B, 1111 (1988).

11. J.D. Winefordner, B.W. Smith, and N. Omenetto, *Spectrochim. Acta* 44B, 1397 (1989).

12. J.P. Dougherty, J.A. Costella, and R.G. Michel, *Anal. Chem.* 60(4), 336 (1988).

13. N. Omenetto and J.D. Winefordner, *Appl. Spectrosc.* 26, 555 (1972).

14. C. Van Dijk, B.E. Smith, and J.D. Winefordner, *Spectrochim. Acta* 37B, 759 (1982).

15. G. Kirchoff and R. Dunsen, *Pogg. Ann.* 110, 161 (1860).

16. G. Kirchoff and R. Dunsen, *Pogg. Ann.* 113, 337 (1861).

17. G. Kirchaff and R. Bensen, *Phil. Mag.* 22, 275 (1861).

18. W.H. Wallasten, *Phil. Trans.* 92, 365 (1902).

19. J. Fraunhofer, *J. Ann. Phys.* 56, 264 (1817).

20. R.W. Wood, *Phil. Mag.* 10, 782 (1906).

21. E. Wiedenmann and G.C. Schmidt, *Uber Lumineszenz Ann. d. Phys.* 54, 604 (1895).

22. R.W. Wood, *Phil. Mag.* 10, 513 (1905).

23. R.W. Wood, *Physical Optics*. Dover Publications, New York (1934).

24. P. Pringsheim, *Fluorescence and Phosphorescence*. United Press, New York (1949).

25. A.C.G. Mitchell and M.W. Zemansky, *Resonance Radiation and Excited Atoms*. Cambridge Univ. Press, London (1971).

26. E.L. Nichols and H.L. Howes, *Phys. Rev.* 22, 425 (1923).

27. R.M. Badger, *Z. Phys.* 55, 56 (1929).

28. A.L. Boers, C.Th.J. Alkemade, and J.A. Imit, *Physica* 22, 358 (1956).

29. *Proc. 10th Coll. Spectrosc. Int., Maryland* 1962, p. 145. Spartan Books, Washington, DC (1963).

30. J.D. Winefordner and T.J. Vickers, *Anal. Chem.* 36, 161 (1964).

31. J.D. Winefordner and R.A. Staab, *Anal. Chem.* 36, 165 (1964).

32. C. Veillon, M.L. Parsons, J.M. Mansfield, and J.D. Winefordner, *Anal. Chem.* 38, 204 (1964).

33. J.D. Winefordner, S.G. Schulman, and T.C. O'Haver, *Luminescence Spectrometry in Analytical Chemistry*. John Wiley, New York (1973).

34. V. Sycha, V. Svoboda, and I. Rubeska, *Atomic Fluorescence Spectroscopy*. Van Nostrand Reinhold, London (1975).

35. G.F. Kirkbright and M. Sargent, *Atomic Absorption and Fluorescence Spectroscopy*. Academic Press, London (1974).

36. J.D. Winefordner and J. M. Mansfield, "Atomic Fluorescence Flame Spectrometry," in: *Fluorescence,* Ed. G.G. Gilbrant, Vol.1, Chap.2, p. 10. Delken, New York (1967).

37. J.D. Winefordner and J.M. Mansfield, Jr., *Appl. Spectrosc. Rev.* 1, 1 (1967).

38. J.D. Winefordner, V. Svoboda, and L.J. Cline, *CRC Crit. Rev. Anal. Chem.* 1, 233 (1970).

39. T.S. West and M.S. Cresser, *Appl. Spectrosc. Rev.* 7, 79 (1973).

40. J.D. Winefordner, *Rec. Chem. Prog.* 29, 24 (1968).

41. G.F. Kirkbright and T.S. West, *Chem. Brit.* 8, 428 (1972).

42. T.S. West, *Analyst* 99, 886 (1974).

43. R.F. Browner, *Analyst* 99, 617 (1974).

44. N. Omenetto and J.D. Winefordner, *Prog. Analyt. Atom. Spectrosc.* 2, 1 (1979).

45. J.D. Winefordner and R.C. Elsner, *Anal. Chem.* 43(4), 24A (1971).

46. J.D. Winefordner, *Accounts Chem. Res.* 4, 259 (1971).

47. J.D. Winefordner, *J. Chem. Ed.* 55, 72 (1978).

48. J.D. Winefordner, *Chemtech.* 123, 10 (1975).

49. D.J. Butcher, J.P. Dougherty, J.T. McCaffrey, F.R. Preli, Jr., and A.P. Walter, *Appl. Spectrosc.* 41, 359 (1987).

50. J.D. Winefordner, "Atomic Fluorescence Spectrometry; Past Present, and Future," in: *Recent Advances in Analytical Spectroscopy*, Ed. K. Fuwa, Vol. 1, Chap. 4, p. 121. Pergamon Press, Oxford (1982).

51. L.M. Fraser and J.D. Winefordner, *Anal. Chem.* 43, 1693 (1971).

52. M.B. Denton and H.V. Malmstadt, *Appl. Phys. Letters* 18, 485 (1971).

53. N. Omenetto, P. Benetti, L.P. Hort, J.D. Winefordner, and C. Alkemade, *Spectrochim. Acta* 28B, 289 (1973).

54. J. Kuhl, S. Newmann, and M. Kriese, *Z. Naturforsch Feil.* 28A, 273 (1973).

55. A.B. Rodrigo and R.M. Measures, *IEEE J. Quantum Electro.* QE-9, 972 (1973).

56. A.P. Baronauski and J.R. McDonald, *Appl. Opt.* 16, 1897 (1977).

57. A.C. Eckbreth, P.A. Bonczyk, and J.A. Shirley, *Investigation of Saturated Laser Fluorescence and CARS Spectroscopic Techniques for Combustion Diagnostics*. EPA-600/7-78-104, June (1978).

58. B.W. Smith, J.D. Winefordner, and N. Omenetto, *J. Appl. Phys.* 48, 2676 (1977).

59. B.L. Sharp and T.J. Goldwesser, *Spectrochim. Acta* 31B, 431 (1976).

60. V. Svoboda, "Investigation on Atomic Fluorescence using Evaporation from a Graphite Crucible." Paper presented to the 1st conference on Atomic Absorption Spectroscopy, Prague, Czech. 1967.

61. H. Massmann, *Spectrochim. Acta* 23B, 215 (1968).

62. *Proc. 13th Coll. Spectrosc. Int., Ottawa* 1967, p. 284. Hilger, London (1968).

63. L.M. Fraser and J.D. Winefordner. "Laser Excited Atomic Fluorescence." Paper presented to the 9th National Meeting of the Society for Applied Spectroscopy, New Orleans (1970).

64. M.A. Bolshov, A.V. Zybin, and I.I. Smirenkum, *Spectrochim. Acta* 36B, 1143 (1981).

65. J.P. Dougherty, F.R. Preli, Jr., and R.G. Michel, *J. Anal. At. Spectrom.* 2, 429 (1987).

66. H. Falk, H.J. Paetzold, K.P. Schmidt, and J. Filch, *Spectrochim. Acta* 43B, 1101 (1988).

67. D. Goforth and J.D. Winefordner, *Anal. Chem.* 58, 2598 (1986).

68. D. Goforth and J.D. Winefordner, *Talanta* 34, 290 (1987).

69. N. Omenetto, P. Cavalli, M. Braglia, P. Qu, and G. Rossi, *J. Anal. At. Spectrom.* 3, 231 (1988).

70. J.A. Vera, M.B. Leong, N. Omenetto, B.W. Smith, J.B. Womack, and J.D. Winefordner, *Spectrochim. Acta* 44B, 10 (1989).

71. A. Montaser and V.A. Fassel, *Anal. Chem.* 48, 1490 (1976).

72. D.R. Demers and C.D. Alemand, *Anal. Chem.* 53, 1915 (1981).

73. M.S. Epstein, S. Nikdel, N. Omenetto, R.D. Reeves, J.D. Bradshaw, and J.D. Winefordner, *Anal. Chem.* 51, 2071 (1979).

74. N. Omenetto and J.D. Winefordner, *Radiative Chemistry: Principles and Application*. VCH Publishers, New York (1987).

75. F. Llewellyn-Jones, *The Glow Discharge*. John Wiley, New York (1966).

76. F. Paschen, *Ann. Phys*. 50, 901 (1916).

77. F. Paschen, *Ann. Phys*. 71, 142 (1923).

78. R.A. Sawyer and F. Pashen, *Ann. Phys*. 84, 1, (1927).

79. R. Frerichs, *Ann. Phys*. 85, 362 (1928).

80. Y. Takahashi, *Ann. Phys*. 3, 49 (1928).

81. R.A. Sawyer, *Phys. Rev*. 36, 44 (1930).

82. V.A. Kanovalov and E.S. Frisch, *Zh. Tekh. Fig*. 4, 523 (1947).

83. H. Schuler, *Z. Phys*. 72, 423 (1931).

84. H. Schuler and H. Gollnow, *Z. Phys*. 93, 611 (1934).

85. J.R. McNally, Jr., G.R. Harrison, and E. Rowe, *J. Opt. Soc. Am*. 37, 93 (1947).

86. F.T. Birks, *Spectrochim. Acta* 4, 85 (1950).

87. V.A. Gromov, *Opt. Specktrosk*. 1, 334 (1956).

88. A. Walsh, *Spectrochim. Acta* 7, 108 (1955).

89. P.F. Little and A.V. Engel, *Proc. R. Soc. London* 224A, 209 (1954).

90. H.M. Crosswhite, G.H. Dieke, and C.S. Legagneur, *J. Opt. Soc. Am.* 45, 270 (1955).

91. D.J. Sturges and H.J. Oskam, *J. Appl. Phys.* 37, 2405 (1966).

92. H. Falk, *Ann. Phys.* 16, 160 (1965).

93. S. Caroli, *Preg. Analyt. Atom Spectrosc.* 6, 253 (1982).

94. S. Caroli, *J. Anal. Atom Spect.* 2, 661 (1987).

95. B.J. Russell and A. Walsh, *Spectrochim. Acta* 15, 883 (1959).

96. B.M. Gatehouse and A. Walsh, *Spectrochim. Acta* 16, 602 (1960).

97. W. Grimm, *Naturwiss.* 54, 586 (1967).

98. W. Grimm, *Spectrochim. Acta* 23B, 443 (1968).

99. B.W. Gandrud and R.K. Skogerboe, *Appl. Spectrosc.* 25, 243 (1971).

100. N.P. Ivanov, M.N. Gasinskii, and A.D. Esikov, *Z. Analit. Khim.* 20, 1133 (1965).

101. Yu. Yokoyama and S. Ikeda, *Spectrochim. Acta* 24B, 117 (1969).

102. *Proc. 15th Coll. Spectrosc. Int., Madrid* 1969, p. 269. Iberica, Madrid (1970).

103. H. Massmann, *Spectrochim. Acta* 25B, 393 (1970).

104. D.S. Gough, P. Hannaford, and A. Walsh, *Spectrochim. Acta* 28B, 197 (1973).

105. D.S. Gough and J.R. Meldrum, *Anal. Chem.* 52, 642 (1980).

106. C. van Dijk, B.W. Smith, and J.D. Winefordner, *Spectrochim. Acta* 37B, 759 (1982).

107. B.W. Smith, N. Omenetto, and J.D. Winefordner, *Spectrochim. Acta* 39B, 1389 (1985).

108. B.M. Patel, B.W. Smith, and J.D. Winefordner, *Spectrochim. Acta* 40B, 1195, (1984).

109. B.W. Smith, J.B. Womack, N. Omenetto, and J.D. Winefordner, *J. Appl. Spectrosc.* 43, 873 (1989).

110. M. Glick, B.W. Smith, and J.D. Winefordner, *Anal. Chem.* 62(2), 157 (1990).

111. B.V. L'vov, *Atomic Absorption Spectrochemical Analysis*. Hilger, London (1970).

112. C.Th.J. Alkemade, T.J. Hollander, W. Snellman, and P.J.Th. Zeegers, *Metal Vapors in Flames*. Pergamon Press, Oxford (1982).

113. E.H. Piepmeier, *Lasers in Analytical Chemistry*. Hilger, London (1970).

114. N. Omenetto and J.D. Winefordner, *Appl. Spectrosc.* 26(5), 555 (1972).

115. W. Demtröder, *Laser Spectroscopy: Basic Concepts and Instrumentation*. Springer-Verlag, New York (1982).

116. A.P. Thorne, *Spectrophysics*. Chapman and Hall, New York (1988).

117. N. Omenetto and J.D. Winefordner, "Atomic Fluorescence Spectroscopy With Laser Excitation," in: *Analytical Laser Spectroscopy,* Ed. N. Omenetto, Chap. 4, p. 167. John Wiley, New York (1979).

118. N. Omenetto, P. Benetti, L.P. Hort, J.D. Winefordner, and C.Th.J. Alkemade, *Spectrochim. Acta* 28B, 289 (1973).

119. E.H. Piepmeier, *Analytical Applications of Lasers*. John Wiley, New York (1986).

120. O. Svelto, *Principles of Lasers*. Plenum Press, New York (1982).

121. A.E. Siegman, *Lasers*. Univ. Lei. Books, Mill Valley, California (1986).

122. W.T. Walker, N. Solimene, M. Pilch, and G. Gould, *IEEEJ. QE-2*, 474 (1966).

123. R.E. Grove, *Laser Focus Magazine* 18, 45 (1982).

124. F.P. Schafer, *Dye Lasers, Topics in Applied Physics.* Vol. 1, Springer-Verlag, Berlin (1973).

125. T.F. Johnson, Jr., "Tunable Dye Lasers," in: *Encyclopedia of Phys. Sci. and Technol.*, Vol. 14, 96. Academic Press, Orlando, Florida (1987).

126. J. Vera, Ph.D. dissertation, University of Florida, Gainesville, Florida (1989).

127. M.D. Levenson, *Introduction to Nonlinear Laser Spectroscopy*. Academic Press, New York (1982).

128. R.W. Hellworth, *Prog. Quantum Electron*. 5, 1 (1977).

129. S.A.J. Druet and J.P.E. Taran, *Prog. Quantum. Electron*. 7, 1 (1981).

130. W.W. Harrison and B.L. Bentz, *Prog. Analyt. Spectrosc*. 11, 53 (1988).

131. D.F. Hunt, L.N. McEwen, and T.M. Harvey, *Anal. Chem*. 47, 1730 (1975).

132. R.M. Barnes, *Emission Spectroscopy*. Dawden, Hutchinson and Ross, Shandsburg, Pennsylvania (1976).

133. P.W.J.M. Boumans, *Theory of Spectrochemical Excitation*. Hilger and Watts, London (1966).

134. P.A. Linders, W.M. Mulaire, and G.K. Wehner, *Lerf. Cont. Technol*. 29, 275 (1986).

135. J.D. Colune, *Gaseous Conductors, Theory and Engineering Applications*. Dover, New York (1941).

136. G.K. Wehner, "Glow Discharges," in: *Methods and Phenomenon: Their Applications in Science and Technology*. Eds. S.P. Walsky and A.W. Czandema, Chap. 3, p. 231. Elsevier Scientific, New York (1975).

137. S. Caroli, *Prog. Analyt. Spectrosc*. 6, 253 (1983).

138. F. Howorka and M. Pahl, *Z. Naturforsch*. 27A, 1425 (1972).

139. A. Benninghaven, *Surf. Sci*. 53, 596 (1975).

140. G.K. Wehner and G.S. Anderson, "Cathodic Surface Sputtering," in: *Handbook of Thin Film Technology*. Eds. L.I. Maissel and R. Glory, Vol. 2, Chap. 3, p. 160. McGraw-Hill, New York (1970).

141. R.E. Henig, *Adv. Mass Spectrom*. 6, 337 (1974).

142. B.J. Stocker, *Br. J. Appl. Phys.* 12, 465 (1961).

143. T. Musha, *J. Phys. Soc. Japan* 17, 1440 (1962).

144. V. Orlinov, B. Goranchev, and J. Kouster, *Int. J. Electron.* 36, 431 (1974).

145. P. Hannaford, *Centerp. Phys.* 24, 251 (1983).

146. R.J. MacDonald, "The Sputtered Atom Light Source," in: *Recent Advances in Analytical Spectroscopy*. Ed. K. Fuwa, Vol. 1, Chap. 20, p. 249. Pergamon Press, Oxford (1982).

147. J.M. Schroser, R.N. Rhodin, and R.C. Bradley, *Surf. Sci.* 34, 571 (1973).

148. C.G. Bruhn and W.W. Harrison, *Anal. Chem.* 50, 16 (1978).

149. J.W. Coburn, *Rev. Sci. Instrum.* 41, 1219 (1970).

150. G.F. Kirkbright, *Analyst* 96, 609 (1971).

151. J.W. Coburn and E. Kay, *Appl. Phys. Lett.* 18, 435 (1971).

152. W.D. Westwood, *Preg. Surf. Sci.* 7, 71 (1976).

153. H. Kano, T. Shay, and G.J. Collins, *Appl. Phys. Lett.* 27, 610 (1975).

154. M. Hecq, A. Hecq, and M. Fontignies, *Anal. Chim. Acta* 155, 191 (1983).

155. H. Hotop and A. Nickaus, *Z. Physik.* 215, 1395 (1968).

156. K.C. Smyth, B.L. Bentz, C.G. Bruhn, and W.W. Harrison, *J. Am. Chem. Soc.* 101, 797 (1979).

157. H. Oeschner, *Plasma Phys.* 16, 835 (1974).

158. C.L. Stevenson and J.D. Winefordner, *Chemtracts*, May/June (1990) in press

159. C.Th.J. Alkemade, "Counting Atoms With Lasers," in: *Analytical Applications of Lasers*, Ed. E.H. Peipmeier, Chap. 4, p. 261. John Wiley, New York (1986)

160. J. Lotrian, Y. Guern, J. Carion, and A. Johannin-Giles, *J. Quant. Spectrosc. Radiat. Transfer.* 23, 445 (1974)

161. F.R. Preli, Jr., J.P. Dougherty, and R.G. Michel, *Anal Chem.* 49, 1784 (1987)

BIOGRAPHICAL SKETCH

James Benjamin Womack was born in Greenwood, South Carolina, on July 7, 1964. In June 1982, he graduated from Belton-Honea Path High School in Honea Path, South Carolina. In May 1986, he graduated from Erskine College in Due West, South Carolina, with a Bachelor of Science degree in Chemistry, with honors. In August 1986, he entered graduate school at the University of Florida in Gainesville, Florida.

I certify that I have read this study and that in my opinion it conforms to acceptable standards of scholarly presentation and is fully adequate, in scope and quality, as a dissertation for the degree of Doctor of Philosophy.

James D. Winefordner, Chairman
Graduate Research Professor of
Chemistry

I certify that I have read this study and that in my opinion it conforms to acceptable standards of scholarly presentation and is fully adequate, in scope and quality, as a dissertation for the degree of Doctor of Philosophy.

Joseph J. Delfino
Professor of Environmental Engineering
Sciences

I certify that I have read this study and that in my opinion it conforms to acceptable standards of scholarly presentation and is fully adequate, in scope and quality, as a dissertation for the degree of Doctor of Philosophy.

Anna F. Brajter-Toth
Associate Professor of Chemistry

I certify that I have read this study and that in my opinion it conforms to acceptable standards of scholarly presentation and is fully adequate, in scope and quality, as a dissertation for the degree of Doctor of Philosophy.

Richard A. Yost
Professor of Chemistry

I certify that I have read this study and that in my opinion it conforms to acceptable standards of scholarly presentation and is fully adequate, in scope and quality, as a dissertation for the degree of Doctor of Philosophy.

Merle A. Battiste
Professor of Chemistry

This dissertation was submitted to the Graduate Faculty of the Department of Chemistry in the College of Liberal Arts and Sciences and to the Graduate School and was accepted as partial fulfillment of the requirements for the degree of Doctor of Philosophy.

May, 1991

Dean, Graduate School